

# The influence of AGN feedback on star formation in red spiral galaxies

Moreom Akter<sup>a</sup>, Wayne A. Barkhouse<sup>a,\*</sup>, Sandanuwan P Kalawila Vithanage<sup>b</sup>, Gihan L. Gamage<sup>c</sup>, Omar López-Cruz<sup>d</sup>

<sup>a</sup>*Department of Physics and Astrophysics, University of North Dakota, 101 Cornell Street, Grand Forks, 58202, North Dakota, USA*

<sup>b</sup>*Department of Physics, Gettysburg College, Gettysburg, 17325, Pennsylvania, USA*

<sup>c</sup>*Arts and Science Division, New Mexico State University - Alamogordo, Alamogordo, 88310, New Mexico, USA*

<sup>d</sup>*INAOE, Tonantzintla, 72840, Puebla, Mexico*

---

## Abstract

We investigated the influence of Active Galactic Nuclei (AGN) feedback on star formation in red spiral galaxies by analyzing a sample of 324 red and 273 blue face-on spirals selected from 115 low-redshift galaxy clusters. This multi-wavelength dataset combines optical emission line data from the Sloan Digital Sky Survey with X-ray fluxes from *Chandra* and *XMM-Newton* X-ray space telescopes. Using diagnostic emission line ratios, we constructed Baldwin-Phillips-Terlevich (BPT) diagrams, introduced in 1981 to classify galaxies based on nuclear activity. Our analysis reveals that most red spirals exhibit AGN or low-ionization nuclear emission-line region (LINER) signatures, based on optical data, as determined by their location in the BPT, Cid Fernandes, and Mazzolari diagrams. These results are consistent with the presence of negative feedback from AGNs quenching star formation. Conversely, X-ray analysis reveals that many blue spirals exhibit high X-ray luminosities and are situated in the AGN region of emission line ratio diagrams, suggesting that AGN-driven positive feedback may be enhancing star formation. Our findings support the hypothesis that AGN feedback plays a key role in the evolution of spiral galaxies, particularly in quenching star formation and driving the transition from blue to red spiral systems.

*Keywords:* galaxies: active – galaxies: nuclei – galaxies: spiral – galaxies - star formation

---

## 1. Introduction

Active galactic nuclei (AGN) are among the most luminous and energetic phenomena in the Universe, powered by the accretion of matter and gas onto supermas-

---

\*Corresponding author

*Email addresses:* ma25u@fsu.edu (Moreom Akter), wayne.barkhouse@und.edu (Wayne A. Barkhouse), skalawil@gettysburg.edu (Sandanuwan P Kalawila Vithanage), glgamage@nmsu.edu (Gihan L. Gamage), omarlx@inaoep.mx (Omar López-Cruz)

sive black holes (SMBHs) at the center of galaxies (e.g., [Shakura & Sunyaev, 1973](#); [Kormendy & Ho, 2013](#); [Peterson, 2013](#)). These processes release energy across the electromagnetic spectrum ([Shang et al., 2011](#); [Padovani et al., 2017](#)), and AGNs are recognized as drivers of galaxy evolution through feedback mechanisms that regulate star formation (e.g., [Bower et al., 2006](#); [Fabian, 2012](#); [Silk, 2013](#); [Zinn et al., 2013](#); [Dubois et al., 2016](#); [Stemo et al., 2020](#); [Yao et al., 2021](#)). Feedback can be either negative, quenching star formation by ejecting or heating gas (e.g., [Luo et al., 2021](#); [Raouf et al., 2024](#); [Rubinur, 2024](#)), or positive, triggering star formation by compressing interstellar matter (e.g., [Masters et al., 2010](#); [Silk, 2013](#); [Wagner et al., 2016](#); [Morganti, 2017](#); [Cresci & Maiolino, 2018](#); [Abdulrahman et al., 2023](#); [Venturi et al., 2023](#)).

Spiral galaxies are rich in gas and dust, which fuels the formation of young, massive, hot blue stars, making them appear brighter and bluer than most other galaxy types ([Singh et al., 2013](#)). Spiral galaxies provide a valuable framework for investigating AGN feedback across different evolutionary stages ([van den Bergh, 1998](#)). The placement of galaxies in the color-magnitude diagram (CMD) reveals a bimodal distribution; star-forming blue cloud, quiescent red-sequence, and the transitional green valley (e.g., [Kauffmann et al., 2003](#); [Bell et al., 2004](#); [López-Cruz et al., 2004](#); [Faber et al., 2007](#); [Salim, 2014](#)). Numerous studies have identified an enhanced frequency of AGNs within green valley galaxies, implying that AGN activity may play a direct role in the transitioning of galaxies from blue to red (e.g., [Pierce et al., 2007](#); [Schawinski et al., 2007](#); [Povic et al., 2012](#); [Wang et al., 2017](#); [Lacerda et al., 2020](#)).

The impact of AGNs on galaxy properties is closely tied to structural features such as bars, which are known to drive gas toward galaxy centers and potentially fuel SMBH accretion (e.g., [Diaz-Garcia et al., 2020](#)). However, some studies (e.g., [Noguchi, 1996](#); [Lesser, 2022](#)) argue that bar instabilities alone are not sufficient to explain quenching in red spirals, reinforcing the role of AGNs as regulators of star formation ([Lesser et al. 2026](#), in preparation). Additionally, LINERs (low-ionization nuclear emission-line regions; [Heckman, 1980](#)) are commonly found in the bulges of early-type spiral galaxies, which have a higher fraction of older stars compared to late-type spirals, and can contain low-luminosity AGNs (LLAGN) through shock-ionized gas (e.g., [Heckman, 1980](#); [Ferland & Netzer, 1983](#); [Halpern & Steiner, 1983](#); [Terlevich & Melnick, 1985](#); [Ho et al., 2003](#); [Kauffmann et al., 2003](#)).

Advances in multi-wavelength surveys have significantly improved our ability to identify and classify AGNs. Optical diagnostics such as the BPT diagram (e.g., [Baldwin et al., 1981](#); [Kewley et al., 2001a,b](#); [Kauffmann et al., 2003](#); [Schawinski et al., 2007](#); [Venturi et al., 2023](#); [Mazzolari et al., 2024, 2025](#)) are now routinely complemented with infrared ([Jarrett et al., 2011, 2013](#)), ultraviolet ([Mahajan et al., 2018](#)), and X-ray diagnostics ([Brandt & Alexander, 2015](#)). These multi-wavelength tools are essential for resolving ambiguities in AGN classifications, particularly in obscured systems or galaxies with composite spectra (e.g., [Hickox & Alexander, 2018](#); [Agostino & Salim, 2019](#); [Birchall et al., 2020, 2022](#)).

Recent studies have emphasized that LINER classifications, particularly in the [N II]/H $\alpha$  BPT diagram, may not reliably distinguish AGN-powered emission from ionization due to old stellar populations or shocks ([Cheng et al., 2025](#)). Although [S II] and [O I] yield a better method to discriminate Seyferts and LINERs, the [N II] diagram lacks a unified boundary, leading to misclassification in AGN census studies.

This highlights the need for revised diagnostic criteria, such as the recently proposed Seyfert–LINER demarcation line (Cheng et al., 2025), which improves the consistency of classification between BPT branches.

In this study, we investigate the impact of AGN feedback on star formation using a sample of 324 red and 273 blue spiral galaxies drawn from 115 low-redshift ( $0.012 < z < 0.179$ ) galaxy clusters. Our goal is to test the hypothesis that AGNs can exert both negative and positive feedback on star formation, and thus play a dual role in shaping the evolution of spiral galaxies. In Section 2 we describe our data and sample selection. We present key results from optical emission-line ratio and X-ray analyses in Section 3. The discussion is given in Section 4, and in Section 5 we summarize the conclusions of this study.

We use the Friedmann–Lemaître–Robertson–Walker cosmology with  $H_0 = 70$  km s<sup>-1</sup> Mpc<sup>-1</sup>,  $\Omega_\Lambda = 0.7$ , and  $\Omega_M = 0.3$  throughout this study.

## 2. Data and sample selection

This study is based on a multi-wavelength dataset that includes Sloan Digital Sky Survey (SDSS) optical fiber spectroscopy and X-ray observations, thus providing a wavelength coverage sensitive to multiple emission mechanisms relevant to both nuclear and star-forming activity.

### 2.1. Cluster membership and morphology

Galaxies were selected from a well-defined sample of 115 low-redshift ( $0.012 < z < 0.179$ ) clusters, 14 of which were observed with the 3.6-meter Canada-France-Hawaii Telescope (CFHT) using the MegaCam detector in the  $u$ - and  $r$ -passband, with data reduction, object detection, and galaxy photometry fully described in Rude et al. (2020). In addition,  $B$ - and  $R_c$ -band observations of 31 clusters were obtained with the KPNO 0.9-meter telescope using the T2KA CCD detector and the MOSAIC 8K camera (see López-Cruz et al., 2004; Barkhouse et al., 2007, 2009, for details regarding object detection and photometry). Supplementary archival imaging data and catalogs were included from the WINGS survey (Fasano et al., 2006; Varela et al., 2009; Valentinuzzi et al., 2011), providing  $B$ - and  $V$ -band observations of 70 clusters obtained with the 2.5-meter INT and the MPG/ESO 2.2-meter telescopes (see Moretti et al., 2014, for details regarding catalog and image access).

All galaxy cluster catalogs from the 115-cluster sample have been analyzed in a homogeneous fashion using the same procedure to measure red-sequence slopes,  $y$ -intercepts, and dispersions from cluster color-magnitude diagrams (see López-Cruz et al., 2004, for details regarding the fitting method). The faint-end magnitude cut-off for each cluster is based on the limiting magnitude in the  $r/R_c/V$ -band, where the mean  $2.5\sigma$  color uncertainty in the cluster red-sequence exceeds the  $\pm 3\sigma_d$  dispersion of the red-sequence. The red-sequence dispersion ( $\sigma_d$ ) is measured by a Gaussian fit to the color-magnitude distribution (López-Cruz et al., 2004; Barkhouse et al., 2007). All galaxies fainter than the limiting magnitude of the host cluster are excluded from further analysis.

To minimize selection effects, red spirals were defined as those that are located within  $\pm 3\sigma_d$  of the red-sequence. Blue spirals are those that are found  $> 3\sigma_d$  blueward

of the red-sequence in the color-magnitude diagram. Spectroscopic redshifts were obtained from SDSS and NASA/IPAC Extragalactic Database (NED) to confirm cluster membership and minimize inclusion of interlopers. Galaxies were included in our sample if their redshifts are within  $\pm 3\sigma_v$  of the cluster velocity dispersion (Yahil & Vidal, 1977) relative to the brightest cluster galaxy (BCG) of the host cluster.

A k-correction was applied to each galaxy based on redshift and color, and was calculated from Chilingarian et al. (2010) and Chilingarian & Zolotukhin (2012). We used  $R_V = 3.1$  for Milky Way extinction corrections (Schlafly & Finkbeiner, 2011), and no correction was made for host galaxy extinction. Only face-on or nearly face-on spirals with obvious spiral arm structures were included to minimize the effect of dust extinction and to preclude the inclusion of edge-on S0 galaxies. Spiral galaxies were selected via visual verification to avoid the inclusion of non-spiral systems.

Our final sample of face-on cluster spiral galaxies consists of 273 blue spirals and 324 red spirals. Based on SDSS DR 17 photometry, extinction- and k-corrected absolute magnitudes  $M_r$  of blue spirals range from  $-17.1 > M_r > -23.0$ , with an average of  $-21.2$ , while red spirals range from  $-17.3 > M_r > -23.3$ , with a mean of  $-21.2$ . The average redshift of our sample of blue spirals is  $z = 0.076$ , while the average for red spiral galaxies is  $z = 0.067$ .

Using the relationship between  $M_r$  and galaxy mass given by Mahajan et al. (2018, see their Figure 2), the mass of blue spirals range from  $2.4 \times 10^8 M_\odot$  to  $1.3 \times 10^{11} M_\odot$ . The mass range of red spirals extends from  $3.0 \times 10^8 M_\odot$  to  $1.8 \times 10^{11} M_\odot$ .

## 2.2. SDSS optical spectroscopy

Optical fiber spectroscopy data were obtained from the MPA-JHU and SDSS DR18 value-added catalogs (for details, see York et al., 2000; Brinchmann et al., 2004; Tremonti et al., 2004; Almeida et al., 2023) using standard  $S/N \geq 3$  cuts for reliability. MPA-JHU spectral measurements have been corrected for galactic extinction and reddening. Emission-line fluxes were extracted for [O III]  $\lambda\lambda 5007 \text{ \AA}$ ,  $4363 \text{ \AA}$ ; [N II]  $\lambda 6584 \text{ \AA}$ ; [S II]  $\lambda\lambda 6717 \text{ \AA}$ ,  $6731 \text{ \AA}$ ; [O I]  $\lambda 6300 \text{ \AA}$ ; [O II]  $\lambda\lambda 3726 \text{ \AA}$ ,  $3729 \text{ \AA}$ ; [Ne III]  $\lambda 3869 \text{ \AA}$ ; [He II]  $\lambda 4686 \text{ \AA}$ ,  $H\alpha$ ,  $H\beta$ , and  $H\gamma$ . These measurements were used to construct emission-line diagnostic diagrams for classifying AGN and star-forming galaxies. Although SDSS galaxy spectroscopy is obtained using  $3''$  diameter fibers centered on each measured galaxy, this ‘‘aperture bias’’ is expected to have minimal impact on our results since we are probing the contribution to star formation from AGNs that are located in the central regions of galaxies. For the redshift range of our sample ( $0.012 < z < 0.179$ ), a  $3''$  diameter fiber corresponds to a physical size of 0.8 kpc to 9.0 kpc.

## 2.3. Chandra and XMM-Newton X-ray data

Publicly available X-ray data from the *Chandra X-ray Observatory* Source Catalog Release 2 Series (<https://doi.org/10.25574/csc2>; Evans et al., 2024) and the *XMM-Newton* X-ray space telescope archive were matched to galaxy positions using a  $2''$  search radius. When multiple matches were found, the closest match in position was used. Luminosities were calculated from fluxes in the 0.1–10 keV (*Chandra*) and 0.2–12 keV (*XMM-Newton*) bands using  $L_X = 4\pi D_L^2 F (1+z)^{\gamma-2}$ , where  $D_L$  is the luminosity distance,  $F$  is the observed flux,  $z$  is the redshift, and  $\gamma = 1.7$  (based on Lehmer et al.,

2016; Birchall et al., 2022). When a galaxy was matched in both *Chandra* and *XMM-Newton* catalogs, the flux measurement with the smallest uncertainty was retained. This occurred for 12 out of 45 galaxies, with a difference in flux exceeding  $3\sigma$  for two of the 12 galaxies ( $10.2\sigma$  and  $5.7\sigma$ , see Appendix A, Figure A.1).

Matching our sample to X-ray data yielded a detection for 23 (7.1%) red spirals and 22 (8%) blue spirals. Non-detections of the remaining spirals (552 out of 597, 92.5%) was due to both a lack of coverage by *Chandra* and *XMM-Newton* telescopes (239 spirals out of 597, 40%), and coverage but no detection due to sensitivity limits (313 out of 597, 52.4%). For red spirals, X-ray luminosities range from  $4.342 \times 10^{39}$  erg s<sup>-1</sup> to  $9.950 \times 10^{42}$  erg s<sup>-1</sup>, with a mean of  $5.796 \times 10^{41}$  erg s<sup>-1</sup> and a dispersion (rms) of  $3.062 \times 10^{41}$  erg s<sup>-1</sup>. For blue spiral galaxies, X-ray luminosities range from  $4.139 \times 10^{39}$  erg s<sup>-1</sup> to  $5.056 \times 10^{43}$  erg s<sup>-1</sup>, with an average of  $4.670 \times 10^{42}$  erg s<sup>-1</sup> and a dispersion (rms) of  $2.940 \times 10^{42}$  erg s<sup>-1</sup>.

The detection of AGNs using X-ray data is usually based on selecting galaxies that have an X-ray luminosity above a specific threshold. For example, some studies (e.g., Trouille & Barger, 2010; Trouille et al., 2011; Castelló-Mor et al., 2012; Pons & Watson, 2014) used an X-ray luminosity threshold of  $L_X > 10^{42}$  erg s<sup>-1</sup>. In contrast, Pons (2016) used a low luminosity limit of  $L_X > 10^{41}$  erg s<sup>-1</sup> based on their analysis of a subset of AGNs from the 12 Micron Galaxy Survey (Brightman & Nandra, 2011).

For our X-ray-detected galaxy sample, we found that 9 out of 22 blue spirals (40.9%) have X-ray luminosities  $> 10^{41}$  erg s<sup>-1</sup>, with 22.7% (5 out of 22) having luminosities  $> 10^{42}$  erg s<sup>-1</sup>. For the red spirals, 39.1% (9 out of 23) have luminosities  $> 10^{41}$  erg s<sup>-1</sup> and 4.3% (1 out of 23) have luminosities  $> 10^{42}$  erg s<sup>-1</sup>. Figure 1 shows the distribution of X-ray luminosity for our sample of blue and red spiral galaxies.

### 3. Results

In this section, we describe the results of using optical emission-line diagnostic diagrams and X-ray luminosity analysis to evaluate the effects of possible AGN feedback on star formation in red and blue spiral galaxies located in low-redshift clusters.

#### 3.1. [O III]/H $\beta$ vs [N II]/H $\alpha$

Optical emission-line diagnostic diagrams are widely used to classify galaxies based on their dominant ionization source. One of the most established method is the use of the BPT diagram, which utilizes the ratios [O III]/H $\beta$  versus [N II]/H $\alpha$  to distinguish AGN from star-forming galaxies. This diagnostic diagram is particularly effective because AGNs typically exhibit an elevated [O III]/H $\beta$  ratio due to the presence of high-energy photons ( $>35$  eV) needed for [O III] emission, which are more common in AGN continua than in stellar photoionization (Baldwin et al., 1981).

Additionally, AGNs often have a stronger [N II]/H $\alpha$  ratio compared to normal star-forming galaxies (Veilleux & Osterbrock, 1987). The physical origin of this enhancement lies in the hardness of the AGN radiation field. While young O- and B-type stars in star-forming galaxies produce a relatively soft ionizing spectrum that is rapidly absorbed, AGNs generate a hard power-law continuum extending into the extreme-UV and X-ray regime (Baldwin et al., 1981; Ho, 2008). These high-energy

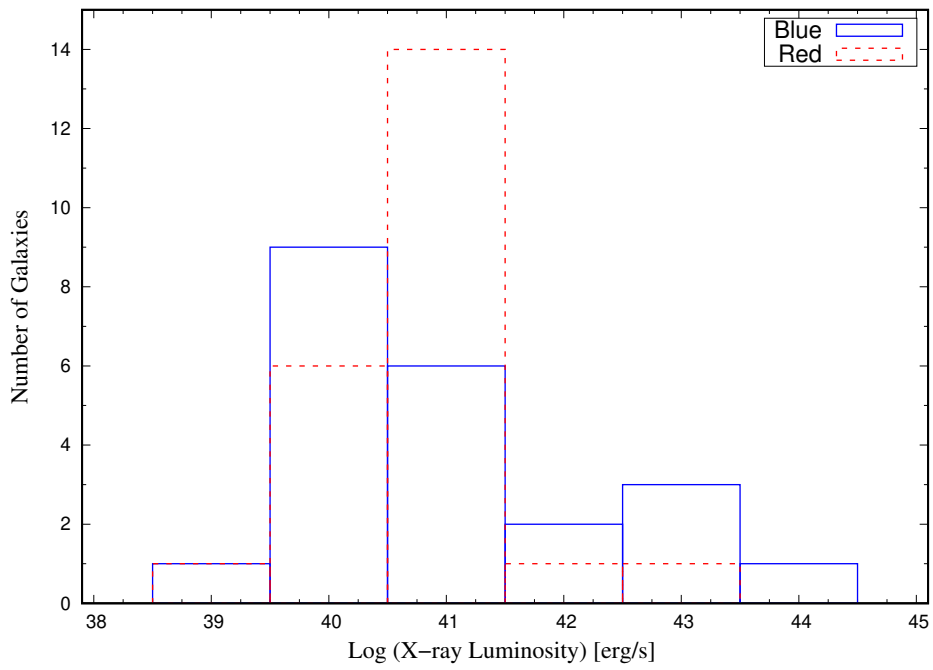


Figure 1: X-ray luminosity histogram distributions for blue (solid boxes) and red cluster spiral galaxies (dashed boxes).

photons penetrate deep into the surrounding interstellar medium, creating extended partially ionized zones where neutral hydrogen and  $N^+$  ions coexist (Ferland & Netzer, 1983; Kewley et al., 2019). In such regions, energetic electrons efficiently collisionally excite nitrogen ions, significantly boosting the [N II]  $\lambda 6584$  emission relative to the recombination-dominated  $H\alpha$  line. This effect can be further enhanced by shocks driven by AGN outflows or jets, which heat and compress the gas and increase the efficiency of low-ionization line emission (Heckman, 1980; Rich et al., 2011; Farage et al., 2010). In contrast, H II regions dominated by stellar photoionization have much thinner partially ionized zones and lack strong shock excitation, resulting in the characteristically lower [N II]/ $H\alpha$  ratios observed in star-forming galaxies.

Figure 2 shows the distribution of galaxies in the standard BPT diagram using the emission-line ratios [O III]/ $H\beta$  versus [N II]/ $H\alpha$ , enabling classification into star-forming, AGN/Seyfert, and LINERs. We note that we use “AGN/Seyfert” in our figures to avoid specific AGN subtype classifications. The black curve and straight line are from Kauffmann et al. (2003), which separates star-forming, AGN/Seyfert, and LINER regions. For the star-forming region, we find that 79.4% of blue galaxies (81 out of 102) occupy this region, while only 15.5% of red galaxies (11 out of 71) are found in this area. In the AGN/Seyfert zone, 18.6% (19) of blue galaxies and 64.8% (46) of red spirals are located in this area. Lastly, in the LINER region we find 2% (2) of blue spirals and 19.7% (14) of red galaxies occupy this area. The number and percent of blue and red galaxies that occupy specific regions of the diagram are tabulated in Table 1, along with the results for other emission-line diagnostic diagrams.

### 3.2. [O III]/ $H\beta$ vs. [S II]/ $H\alpha$

To further refine galaxy classification, we employed the Veilleux & Osterbrock diagrams (hereafter VO87 diagrams; see, for example, Figure 3), which depict alternative line ratios: [O III]/ $H\beta$  vs. [S II]/ $H\alpha$  (Veilleux & Osterbrock, 1987)<sup>1</sup>. This diagram is especially useful for separating narrow-line AGNs from H II region-like galaxies and are sensitive to LINERs, which are often associated with weak AGNs or shock excitation (e.g., Heckman, 1980; Terlevich & Melnick, 1985).

For Figure 3, we find 93.4% (85 out of 91) of blue galaxies are located in the star-forming region, while 3.3% (3) are found each in the AGN/Seyfert and LINER sections. For red spirals, 27.8% (15 out of 54) are in the star-forming area, while 5.6% (3) are classified as AGN/Seyfert and 66.7% (36) are LINER galaxies.

### 3.3. [O III]/ $H\beta$ vs. [O I]/ $H\alpha$

In Figure 4, we use the VO97 diagram of [O III]/ $H\beta$  vs. [O I]/ $H\alpha$  to help separate AGN/Seyfert galaxies from star-forming and LINER-like systems. For Figure 4, we find that 25 out of 31 blue spirals (80.6%) are located in the star-forming region, 12.9% (4) are found in the AGN/Seyfert zone, and 6.4% (2) are in the LINER area. For the red spiral population, only 4.8% (2 out of 42) are star-forming, 11.9% (5) are classified as AGN/Seyfert, and 83.3% (35) are in the LINER region.

---

<sup>1</sup>[S II] = (6717 + 6731) Å and [O II] = (3726 + 3729) Å

In our sample, classification using the schemes of [Dopita et al. \(2000\)](#), [Kewley et al. \(2001a\)](#), [Kewley et al. \(2001b\)](#), [Kauffmann et al. \(2003\)](#), [Kewley et al. \(2006\)](#), [Mazzolari et al. \(2024, 2025\)](#), and [Scholtz et al. \(2025\)](#) shows that most red spirals and a few blue spirals are identified as AGNs in the [N II]/H $\alpha$  BPT diagram. Meanwhile, many of these same galaxies fall into the LINER regions in the VO87 diagrams, supporting the presence of hard ionizing sources such as AGNs or shocks.

Conversely, blue spirals are predominantly distributed across the star-forming regions, suggesting that their ionization is mainly due to young stars, with minimal AGN contribution. Their lower [O III]/H $\beta$  ratios indicate softer ionizing spectra, consistent with stellar photoionization. In contrast, red spirals exhibit systematically higher [O III]/H $\beta$ , [N II]/H $\alpha$ , and [S II]/H $\alpha$  ratios, consistent with harder ionization fields and LINER-like excitation.

### 3.4. [O III] $\lambda 4363/H\gamma$ vs. [O III] $\lambda 5007/[O II]$

We incorporated newer diagnostics proposed by [Mazzolari et al. \(2024, 2025\)](#) and [Backhaus et al. \(2025\)](#), including [O III]  $\lambda 4363/H\gamma$  vs. [O III]  $\lambda 5007/[O II]$ . Figure 5 shows that many red spirals have high [Ne III]/[O II] and [O III]/[O II] ratios, indicative of AGN-like hard ionization. In Figure 5, 0% of blue spirals (0 out of 10) are found in the “star-forming or AGN/Seyfert” region, while only 2.9% (2 out of 68) of red spirals are location in this section of the diagram. Conversely, 100% (10) of blue spirals and 97% (66) of red galaxies are in the “AGN/Seyfert-only” section.

### 3.5. [O III] $\lambda 4363/H\gamma$ vs. [Ne III]/[O II]

An additional diagnostic plot proposed by [Mazzolari et al. \(2024, 2025\)](#) and [Backhaus et al. \(2025\)](#) is the use of [O III]  $\lambda 4363/H\gamma$  vs. [Ne III]/[O II] to help discriminate between star-forming galaxies and AGN/Seyfert systems. Our data are plotted in Figure 6, where 11.1% of blue spirals (1 out of 9) are in the “star-forming” zone, 11.1% (1) in the “SF or AGN/Seyfert” section, and 77.8% (7) are found in the “AGN/Seyfert-only” region. For red spirals, 3.6% (2 out of 56 galaxies) are located in the “star-forming” area, 30.3% (17) in the “SF or AGN/Seyfert” zone, and 66.1% (37) in the “AGN/Seyfert-only” section.

### 3.6. [O III]/[O II] vs. [N II]/H $\alpha$

For sources with incomplete or low S/N in classical emission-line ratio diagrams, we adopted the WHAN-like<sup>2</sup> extension [O III]/[O II] vs. [N II]/H $\alpha$  as shown in Figure 7 ([Cid Fernandes et al., 2010](#)). This plot reveals AGN or LINER-like activity in galaxies misclassified by BPT due to weak lines or dust. In Figure 7, we find that 85 of 97 blue spirals (87.6%) occupy the star-forming region of the figure, 8.2% (8) are AGN/Seyfert, and 4.1% (4) are classified as LINERs. For red spirals, 29.3% (22 of 75 galaxies) are in the star-forming area, 32% (24) are in the AGN/Seyfert zone, and 38.7% (29) are located in the LINER region.

---

<sup>2</sup>The WHAN diagram, introduced by [Cid Fernandes et al. \(2010, 2011\)](#), combines the H $\alpha$  equivalent width with the [N II]/H $\alpha$  ratio to classify galaxies and to include weak-line systems that are excluded from classical BPT diagrams due to low H $\beta$  or [O III] signal-to-noise.

### 3.7. $[O\ III]/H\alpha$ vs. $[N\ II]/H\alpha$

An additional WHAN-like diagnostic plot uses  $[O\ III]/H\alpha$  vs.  $[N\ II]/H\alpha$  to help separate star-forming, AGN/Seyfert, and LINER systems (see Figure 8). Of the 95 blue galaxies plotted in Figure 8, 92.6% (88 out of 95) are located in the star-forming region, 7.4% (7) are AGN/Seyfert, and 0% are LINER. For 62 red spirals, 24.2% (15) are classified as star-forming, 59.7% (37) are in the AGN/Seyfert region, and 16.1% (10) are LINERs.

### 3.8. Equivalent width of $H\alpha$ versus $[N\ II]/H\alpha$

To address galaxies with low S/N in  $H\alpha$  or  $[N\ II]$ , we used the WHAN diagram shown in Figure 9, using the equivalent width (EW) of  $H\alpha$  versus  $[N\ II]/H\alpha$ , to distinguish between strong/weak AGNs, star-forming, retired, and passive galaxies (see for details; Cid Fernandes et al., 2010, 2011). Several red spirals classified ambiguously in BPT were confirmed as LINERs in WHAN, particularly those with  $H\alpha$  EW  $< 3\ \text{\AA}$ . Of the 155 blue spiral galaxies, 74.8% (116) are “pure star-forming,” 14.2% (22) are “strong AGN,” only 1.3% (2) are “weak AGN,” 9.0% (14) are “retired galaxies,” and 0.6% (1) are classified as “passive galaxies.” Of the 114 red spiral galaxies, 15.8% (18) are pure star-forming, 7.9% (9) are strong AGN, 7.0% (8) are weak AGN, 41.2% (47) are retired galaxies, and 28.1% (32) are passive galaxies.

Table 1 presents a summary of galaxy classification based on the emission-line ratio diagnostic plots. Altogether, multiple emission-line diagnostics support that red spirals more frequently host AGNs or LINERs, while blue spirals are typically star-forming, with some showing composite characteristics suggesting coexistence with star-forming and AGN-like activity.

### 3.9. X-ray emission and AGN identification

To complement optical diagnostics, we examined X-ray luminosities from *Chandra* and *XMM-Newton*. A galaxy was classified as an X-ray AGN if its luminosity exceeded  $10^{42}\ \text{erg s}^{-1}$  (e.g., Trouille & Barger, 2010; Castelló-Mor et al., 2012; Pons, 2016), by which we could distinguish AGN-dominated sources from normal star-forming galaxies (e.g., Fabbiano, 1989; Zezas et al., 1998; Moran et al., 1999).

Among our X-ray-detected galaxy sample, 40.9% of blue spirals (9 out of 22) and 39.1% of red spirals (9 out of 23) exceed  $10^{41}\ \text{erg s}^{-1}$ ; 22.7% of blue (5 out of 22) and 4.3% of red spirals (1 out of 23) have  $L_X > 10^{42}\ \text{erg s}^{-1}$ . This suggests AGNs are not exclusive to quiescent systems, supporting the dual-mode feedback model (e.g., Cresci & Maiolino, 2018; Venturi et al., 2023). In this framework, AGNs operate in two distinct modes based on the energy transfer mechanism. The higher-luminosity AGNs in our blue spiral sample correspond to the “radiative mode” (or quasar mode), where energy is released via radiation or winds from the accretion disk, ionizing and heating the surrounding gas (Morganti, 2017). This process regulates star formation by preventing gas from cooling or by expelling it through quasar-driven winds (Harrison et al., 2014; Rubinur, 2024). Conversely, the X-ray activity in our red spirals likely represents the “kinetic mode” (or radio mode), dominant in lower-power AGNs where mechanical energy is injected into the medium via jets and shocks (Morganti, 2017). The presence of significant X-ray luminosities across both populations indicates

that AGN feedback is a multi-stage process, transitioning from radiative-dominated quenching in gas-rich blue systems to a kinetic-dominated mechanism in quiescent red systems.

Only 35% (113 out of 324) red spirals and 36% (98 out of 273) blue spirals had measurable optical emission lines (see Figures 2 to 9), and most were LINERs or LLAGNs, with weak ionization features (Kauffmann et al., 2003; Silverman et al., 2008). The discrepancy between our X-ray detection rates and optical line measurements suggests that a significant fraction of AGN activity in these spirals is obscured or diluted by host galaxy light, particularly in massive, star-forming systems. Tables 4 and 5 gives the classification of galaxies based on X-ray luminosity and emission-line ratios.

Despite a broader range of X-ray luminosities in blue spirals, we performed a cumulative distribution comparison using the Kolmogorov-Smirnov (K-S) test based on measured  $L_X$  values for red and blue galaxies. The test yielded a K-S statistic of  $D = 0.24$  and a probability of  $P = 49\%$ , suggesting that the two galaxy populations are statistically consistent with being selected from the same parent distribution.

An important result is the partial mismatch between X-ray- and optically-selected AGNs, consistent with the findings by Agostino & Salim (2019), showing that optical diagnostics can miss AGNs in star-forming galaxies due to H II contamination. This highlights the need for multi-wavelength AGN identification strategies.

Although detailed *WISE*-based infrared AGN classification is presented in Paper I (Section 3.3), we include Table 2 here to summarize the X-ray properties of galaxies identified as AGNs in the *WISE* color-color diagram for our sample.

### 3.10. Statistical verification of emission-line distributions

K-S tests were performed to determine whether red spirals are affected more by the presence of AGN compared to blue spirals by measuring the statistical significance that both groups of spirals have the same parent distribution using various emission-line ratios. The results tabulated in Table 3 indicate that based on five of the seven emission-line ratio plots, blue and red spirals are statistically not selected from the same parent population. Only Figure 5 based on  $\log([\text{O III}]/H\gamma)$  vs.  $\log([\text{O III}]/[\text{O II}])$  and Figure 6 using  $\log([\text{O III}]/H\gamma)$  vs.  $\log([\text{Ne III}]/[\text{O II}])$ , indicate that blue and red spirals have properties consistent with selection from the same parent distribution.

## 4. Discussion

Our findings are consistent with the dual role of AGN feedback in spiral galaxies. Optical emission-line diagnostics reveal that a significant fraction (71% to 97%) of red spirals exhibit AGN and LINER signatures, consistent with negative feedback processes that suppress star formation and contribute to quenching. This aligns with previous studies (e.g. Schawinski et al., 2007; Cid Fernandes et al., 2011; Povic et al., 2012), which argue that AGNs are instrumental in transitioning galaxies across the green valley toward the red sequence.

On the other hand, there is a noticeable difference between optical and X-ray AGN classifications for blue spirals. Many optically classified star-forming or composite (star-forming/AGN) galaxies exhibit high X-ray luminosities ( $\log L_X > 10^{41}$  erg s<sup>-1</sup>),

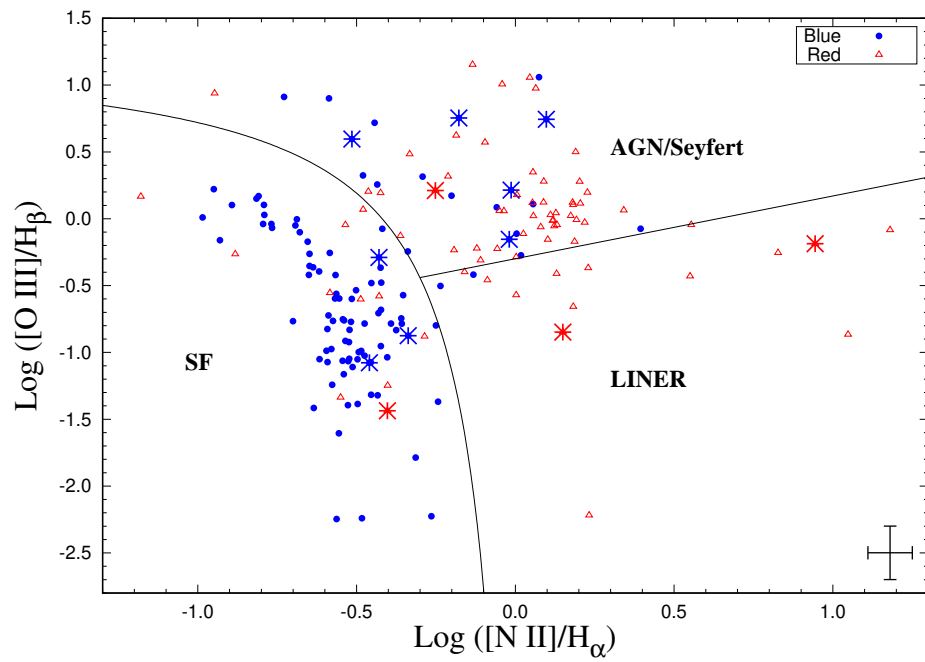


Figure 2: Standard BPT diagram for  $\log ([\text{O III}]/\text{H}\beta)$  vs.  $\log ([\text{N II}]/\text{H}\alpha)$ . Solid curve and straight line are from [Kauffmann et al. \(2003\)](#), which separates AGN/Seyfert, star-forming, and LINER galaxies. Galaxies detected in the X-ray are depicted with asterisk symbols. The median  $1\sigma$  error bars are given in the lower-right corner of the figure.

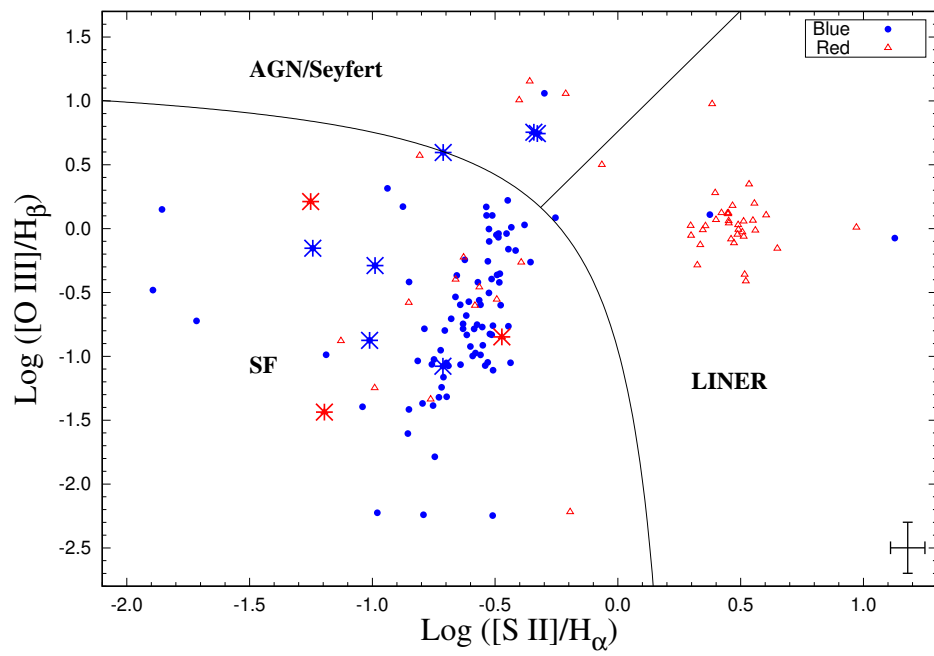


Figure 3: VO87 diagram using  $\log ([\text{O III}]/\text{H}\beta)$  vs.  $\log ([\text{S II}]/\text{H}\alpha)$ . The black curve is from [Kewley et al. \(2001a,b\)](#), which separate the star-forming (SF) region from the AGN/Seyfert area. The straight line, from [Kewley et al. \(2006\)](#), depicts the demarcation line that separate AGN/Seyferts from LINER systems. Galaxies detected in the X-ray are represented by asterisk symbols. The median  $1\sigma$  error bars are given in the lower-right corner of the figure.

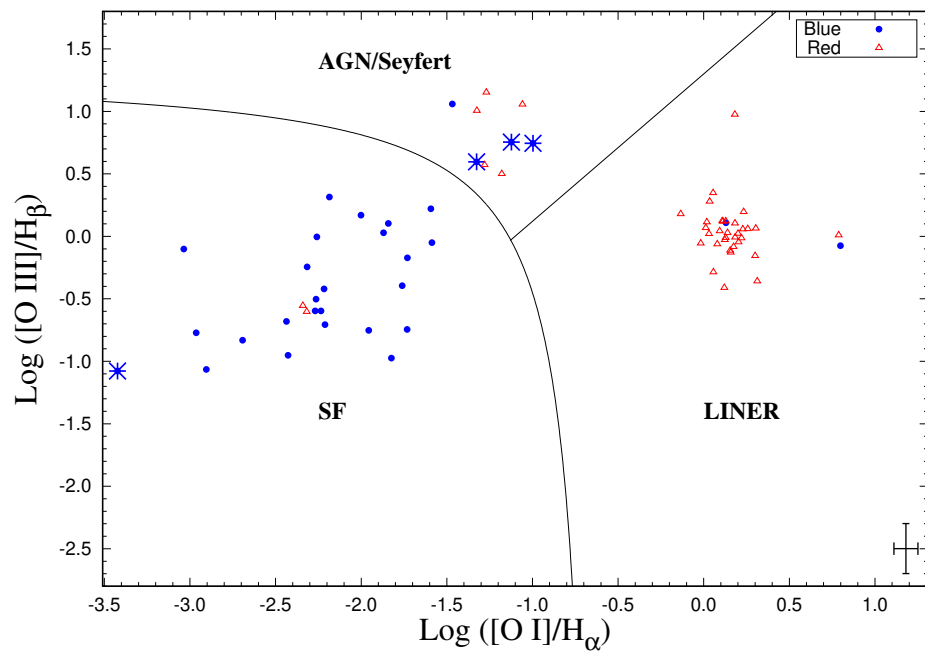


Figure 4: VO87 diagram using  $\log ([\text{O III}]/\text{H}\beta)$  vs.  $\log ([\text{O I}]/\text{H}\alpha)$ . The black curve is from [Kewley et al. \(2001a,b\)](#), which separate the star-forming (SF) region from the AGN/Seyfert area. The straight line, from [Kewley et al. \(2006\)](#), depicts the demarcation line that separate AGN/Seyferts from LINER systems. Galaxies detected in the X-ray are represented by asterisk symbols. The median  $1\sigma$  error bars are given in the lower-right corner of the figure.

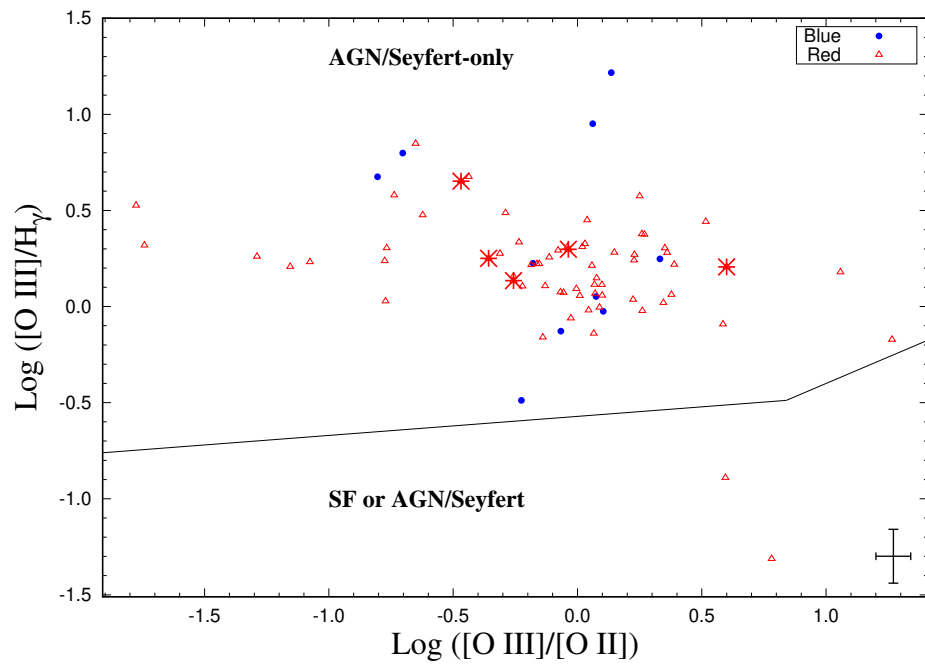


Figure 5: Mazzolari diagram (Mazzolari et al., 2024) plotting  $\log ([\text{O III}]/H\gamma)$  vs.  $\log ([\text{O III}]/[\text{O II}])$ . Straight line segments are from Mazzolari et al. (2024), which separates galaxies into “AGN/Seyfert-only” and “SF or AGN/Seyfert” regions. Galaxies detected in the X-ray are represented by asterisk symbols. The median  $1\sigma$  error bars are given in the lower-right corner of the figure.

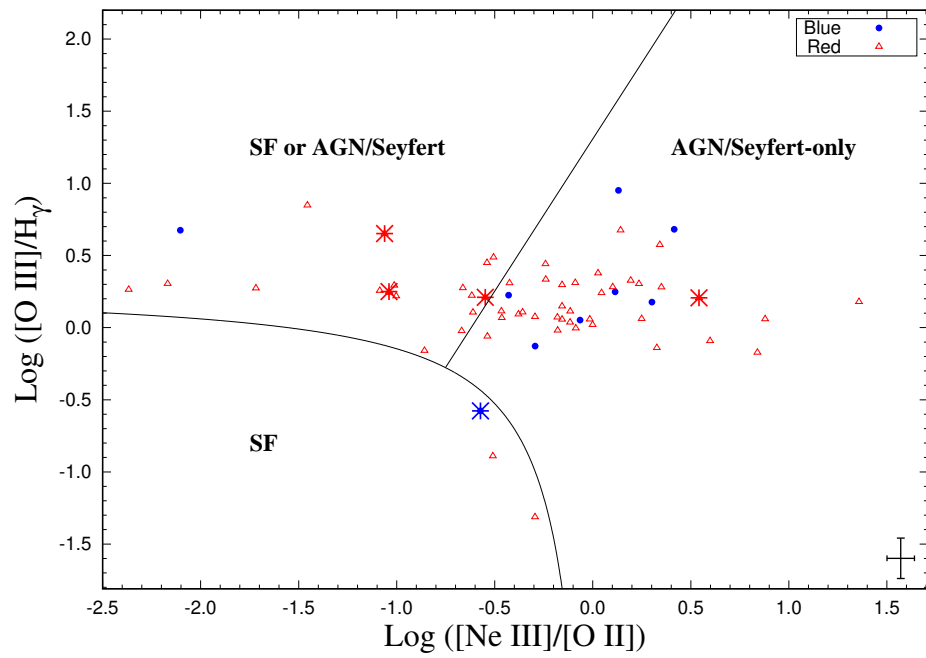


Figure 6: Mazzolari diagram (Mazzolari et al., 2024) using  $\log ([\text{O III}]/\text{H}\gamma)$  vs.  $\log ([\text{Ne III}]/[\text{O II}])$ . The curve and straight lines are from Backhaus et al. (2025), separating “star-forming” (SF), “SF or AGN/Seyfert,” and “AGN/Seyfert-only” regions. Galaxies detected in the X-ray are represented by asterisk symbols. The median  $1\sigma$  error bars are given in the lower-right corner of the figure.

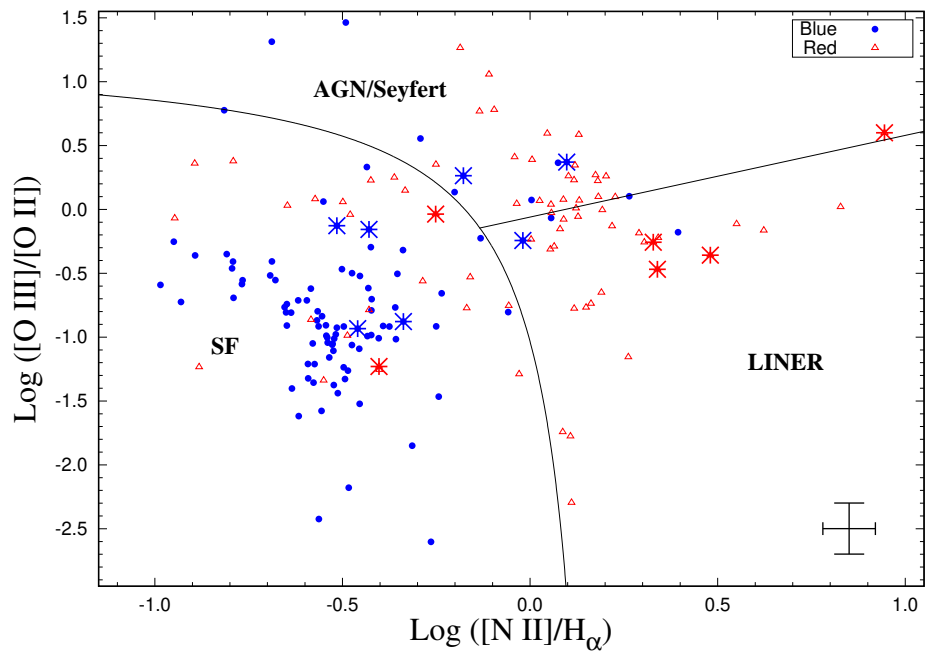


Figure 7: Cid Fernandes diagram (Cid Fernandes et al., 2010) using  $\log ([\text{O III}]/[\text{O II}])$  vs.  $\log ([\text{N II}]/H\alpha)$ . The black curve is from Kewley et al. (2001a,b), which separate the star-forming (SF) region from the AGN/Seyfert area. The straight line, from Kewley et al. (2006), depicts the demarcation line that separate AGN/Seyferts from LINER systems. Galaxies detected in the X-ray are represented by asterisk symbols. The median  $1\sigma$  error bars are given in the lower-right corner of the figure.

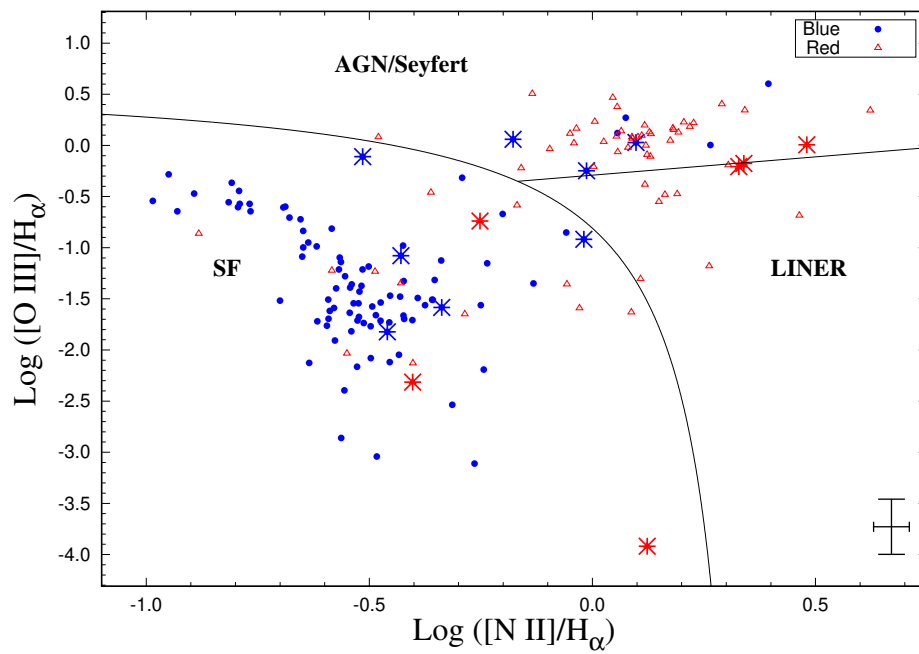


Figure 8: Cid Fernandes diagram (Cid Fernandes et al., 2010) using  $\log([\text{O III}]/\text{H}\alpha)$  vs.  $\log([\text{N II}]/\text{H}\alpha)$ . The black curve is from Kewley et al. (2001a,b), which separate the star-forming (SF) region from the AGN/Seyfert area. The straight line, from Kewley et al. (2006), depicts the demarcation line that separate AGN/Seyferts from LINER systems. Galaxies detected in the X-ray are represented by asterisk symbols. The median  $1\sigma$  error bars are given in the lower-right corner of the figure.

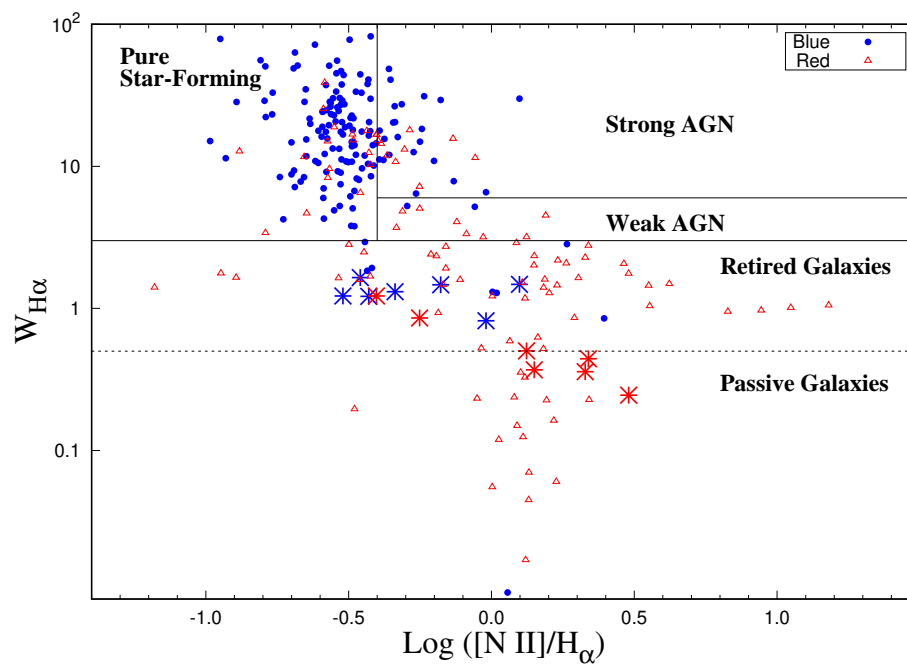


Figure 9: The WHAN diagram from [Cid Fernandes et al. \(2011\)](#) using the equivalent width (EW) of  $H\alpha$  ( $W_{H\alpha}$ ) vs.  $\text{log} ([\text{N II}]/\text{H}\alpha)$ . The horizontal dashed line separates retired and passive galaxies, while the vertical and horizontal solid lines define regions containing pure star-forming, strong, and weak AGN. Galaxies detected in the X-ray are represented by asterisk symbols.

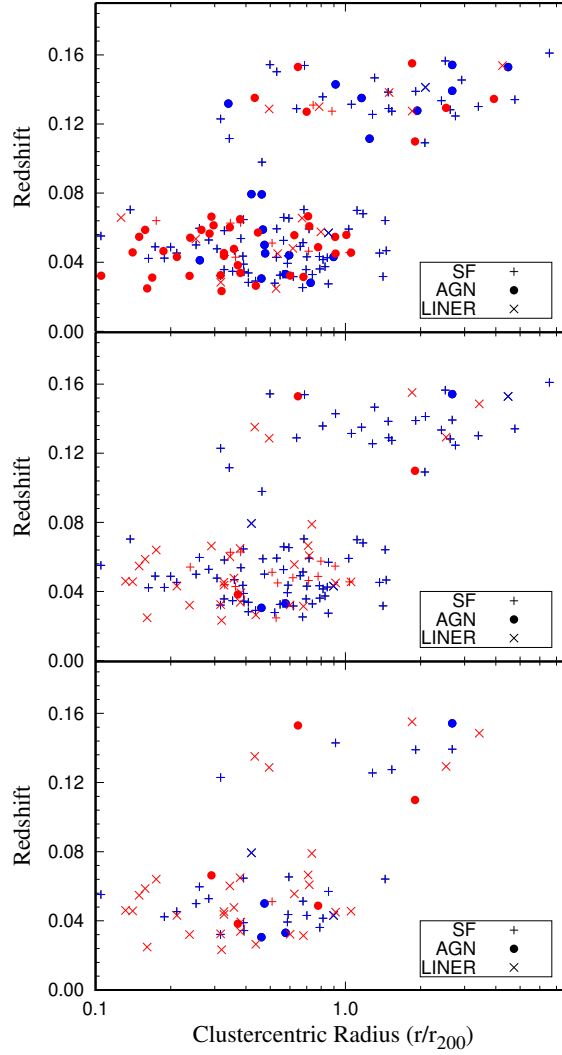


Figure 10: *Top panel:* Redshift versus cluster-centric radius ( $r/r_{200}$ ) for red/blue galaxies classified as “star-forming,” “AGN,” and “LINER” systems based on the standard BPT emission line ratio plot using  $[O III]/H\beta$  vs.  $[N II]/H\alpha$  (see Figure 2). *Middle panel:* Galaxy classification into “star-forming,” “AGN,” and “LINER” systems based on the BPT plot using  $[O III]/H\beta$  vs.  $[S II]/H\alpha$  (see Figure 3). *Bottom panel:* Galaxy classification into “star-forming,” “AGN,” and “LINER” systems based on the BPT plot using  $[O III]/H\beta$  vs.  $[O I]/H\alpha$  (see Figure 4). For all three panels, galaxies classified as “star-forming” are depicted by plus symbols, “AGNs” are denoted by solid circles, and “LINER” galaxies are represented by cross symbols.

suggesting hidden or diluted AGN activity not detectable in the optical regime due to ongoing star formation. This supports findings by both [Hickox et al. \(2009\)](#) and [Birchall et al. \(2022\)](#), who highlight the need for multi-wavelength approaches to fully capture the AGN population, particularly in blue galaxies where star formation masks traditional signatures.

The combination of BPT, WHAN, and alternative diagnostic diagrams (e.g., [Kewley et al., 2001a,b, 2006](#); [Mazzolari et al., 2024, 2025](#); [Backhaus et al., 2025](#)) enhanced the robustness of galaxy classification, revealing the shortcomings of relying solely on a single method. In particular, the WHAN diagram proved valuable in identifying weak or retired AGNs, especially among LINER-classified systems where ionization may arise from post-AGB stars or shocks (e.g. [Cid Fernandes et al., 2011](#)).

In Figure 10, we show the redshift vs. cluster-centric radius ( $r/r_{200}$ ) of red and blue galaxies classified as “star-forming,” “AGN,” and “LINER” systems. In the top panel of Figure 10, galaxy classification is based on the standard BPT plot using  $[\text{O III}]/H\beta$  vs.  $[\text{N II}]/H\alpha$  (see Figure 2). In the middle panel, the  $[\text{O III}]/H\beta$  vs.  $[\text{S II}]/H\alpha$  emission line ratios indicate activity (see Figure 3). Finally, the bottom panel depicts galaxies classified based on activity indicated by  $[\text{O III}]/H\beta$  vs.  $[\text{O I}]/H\alpha$  (see Figure 4). For all three panels, projected cluster-centric distance was normalized to  $r_{200}$  (i.e.,  $r/r_{200}$ ), the radius of a sphere whose density is 200 times the critical density of the universe (cf. [Barkhouse et al., 2007](#)).

Examination of Figure 10 indicates that red spirals that occupy a radius ( $r/r_{200}$ )  $< 2$ , and hence are most likely older cluster members compared to blue spirals at larger cluster-centric distance, have a higher fraction of AGN. Combining galaxy classifications from all three panels in Figure 10, we find that 32% of red spirals with  $(r/r_{200}) < 2$  are AGN, while only 11% of blue spirals selected from within the same radius are AGN. This may be a result of the impact of AGN feedback in helping to transition blue spirals into red systems in galaxy cluster environments ([Martini et al., 2002](#); [Lokas, 2022](#)).

For a complementary analysis of stellar population age and star formation activity, including  $D_n(4000)$  and specific star formation rate metrics, we refer to Paper I ([Barkhouse et al., 2025](#)) which explores the UV and IR properties of our galaxy sample. The  $D_n(4000)$  metric ([Balogh et al., 1999](#)) is a spectral line index constructed from the ratio of the red (measured between 4000 and 4100 Å) to the blue continuum (3850 to 3950 Å). This ratio is sensitive to stellar age and star formation such that a larger value of  $D_n(4000)$  implies a greater stellar population age and a lower star formation rate. The star formation rate is obtained from  $H\alpha$  spectral line measurements and converted to luminosity using galaxy redshift information. The star formation rate is given by  $\text{SFR} (M_\odot \text{ yr}^{-1}) = 7.93 \times 10^{-42} L(H\alpha)$ , where the  $H\alpha$  luminosity,  $L(H\alpha)$ , is in  $\text{erg s}^{-1}$  ([Bell & Kennicutt, 2001](#); [Dhiwar et al., 2023](#)). The specific star formation rate, the star formation rate normalized to galaxy mass, is obtained by dividing the SFR by mass estimated from the extinction- and k-corrected  $M_r$  absolute magnitude of each galaxy ([Mahajan et al., 2018](#)).

These results contribute to the growing evidence that AGNs not only quench but may also stimulate star formation under specific conditions, reinforcing the idea of “positive feedback” (e.g. [Wagner et al., 2016](#); [Venturi et al., 2023](#)). In this study, galaxy environments likely amplify these effects by influencing gas availability and dynamical interactions.

## 5. Conclusions

This study investigates the relationship between AGN feedback and star formation in 597 spiral galaxies from 115 low-redshift galaxy clusters, using a multi-wavelength dataset incorporating optical and X-ray observations. Key findings include:

- A majority of red spiral galaxies (70.7% to 97.0%, depending on the diagnostic, see Table 1) display AGN or LINER signatures in optical diagnostics, consistent with feedback-driven suppression of star formation.
- A significant fraction of blue spirals show high X-ray luminosities, with 40.9% (9 out of 22) having  $L_X \geq 10^{41}$  erg s<sup>-1</sup> and 22.7% (5 out of 22) exceeding  $L_X \geq 10^{42}$  erg s<sup>-1</sup>, despite being classified as star-forming or composite (star-forming/AGN) in optical diagrams, indicating hidden or optically obscured AGN activity.
- The combined use of BPT, WHAN, and extended diagnostics (e.g., [Mazzolari et al., 2024, 2025](#); [Backhaus et al., 2025](#)) improves AGN identification by recovering additional AGNs in galaxies where one or more classical BPT lines are weak or undetected. For galaxies with most of the emission-line coverage, the classical BPT diagram identifies AGN/LINER activity in ~85% of red spirals and ~21% of blue spirals, while extended low-metallicity and low-S/N diagnostics increase the recovered AGN fraction to ~70–100% in red spirals and ~12–100% in blue spirals, demonstrating that extended diagnostics are more efficient for identifying AGNs in emission-line-weak and low-metallicity systems, whereas the classical BPT diagram remains robust for strong-line galaxies.
- The partial mismatch between optical and X-ray classifications, especially in blue spirals, supports the role of multi-wavelength diagnostics to uncover AGNs missed in traditional optical surveys due to dilution by H II regions.
- These results support a dual-mode AGN feedback scenario, where AGNs in red spirals are associated with star formation quenching (negative feedback), while those in blue spirals may contribute to or coexist with ongoing star formation (positive feedback).

## Acknowledgments

This research was partially funded by ND NASA EPSCoR.

This research has made use of the NASA/IPAC Extragalactic Database (NED), which is operated by the Jet Propulsion Laboratory, California Institute of Technology, under contract with the National Aeronautics and Space Administration. This publication makes use of data products from the Wide-field Infrared Survey Explorer ([Wright et al., 2010](#)), which is a joint project of the University of California, Los Angeles, and the Jet Propulsion Laboratory/California Institute of Technology, funded by the National Aeronautics and Space Administration. Based on observations made with the NASA Galaxy Evolution Explorer. GALEX is operated for NASA by the California Institute of Technology under NASA contract NAS5-98034.

This research has made use of data obtained from the Chandra Source Catalog, provided by the Chandra X-ray Center (CXC). Based on observations obtained with XMM-Newton, an ESA science mission with instruments and contributions directly funded by ESA Member States and NASA.

Funding for SDSS-III has been provided by the Alfred P. Sloan Foundation, the Participating Institutions, the National Science Foundation, and the U.S. Department of Energy Office of Science. The SDSS-III website is <http://www.sdss3.org/>. SDSS-III is managed by the Astrophysical Research Consortium for the Participating Institutions of the SDSS-III Collaboration including the University of Arizona, the Brazilian Participation Group, Brookhaven National Laboratory, University of Cambridge, Carnegie Mellon University, University of Florida, the French Participation Group, the German Participation Group, Harvard University, the Instituto de Astrofísica de Canarias, the Michigan State/Notre Dame/JINA Participation Group, Johns Hopkins University, Lawrence Berkeley National Laboratory, Max Planck Institute for Astrophysics, Max Planck Institute for Extraterrestrial Physics, New Mexico State University, New York University, Ohio State University, Pennsylvania State University, University of Portsmouth, Princeton University, the Spanish Participation Group, University of Tokyo, University of Utah, Vanderbilt University, University of Virginia, University of Washington, and Yale University. This research made use of the “K-corrections calculator” service available at <http://kcor.sai.msu.ru/>.

Based on observations obtained with MegaPrime/MegaCam, a joint project of CFHT and CEA/IRFU, at the Canada-France-Hawaii Telescope (CFHT), which is operated by the National Research Council (NRC) of Canada, the Institut National des Science de l’Univers of the Centre National de la Recherche Scientifique (CNRS) of France, and the University of Hawaii.

We thank the reviewer for providing thoughtful comments and suggestions which improved the manuscript.

## References

- Abdulrahman, M.A., Gadallah, K.A.K., Ahmed, A., Elnawawy, M.S., 2023. The impact of the AGN and the torus properties on the evolution of spiral galaxies. *Mon. Notices RAS* 519 (1), 861-870. <https://doi.org/10.1093/mnras/stac3602>.
- Agostino, C.J., Salim, S., 2019. Crossing the Line: Active Galactic Nuclei in the Star-forming Region of the BPT diagram. *Astrophys. J.* 876 (1), 12. <https://doi.org/10.3847/1538-4357/ab1094>.
- Almeida, A., Anderson, S.F., Argudo-Fernández, M., Badenes, C., Barger, K., Barrera-Ballesteros, J.K., Bender, C.F., Benitez, E., Besser, F., Bird, J.C., Bizyaev, D., Blanton, M.R., Bochanski, J., Bovy, J., Brandt, W.N., Brownstein, J.R., Buchner, J., Bulbul, E., Burchett, J.N., Cano Díaz, M., Carlberg, J.K., Casey, A.R., Chandra, V., Cherinka, B., Chiappini, C., Coker, A.A., Comparat, J., Conroy, C., Contardo, G., Cortes, A., Covey, K., Crane, J.D., Cunha, K., Dabbieri, C., Davidson, J.W., Davis, M.C., de Andrade Queiroz, A.B., De Lee, N., M’endez Delgado, J.E., Demasi, S.,

- Di Mille, F., Donor, J., Dow, P., Dwelly, T., Eracleous, M., Eriksen, J., Fan, X., Farr, E., Frederick, S., Fries, L., Frinchaboy, P., Gänsicke, B.T., Ge, J., González Ávila, C., Grabowski, K., Grier, C., Guiglion, G., Gupta, P., Hall, P., Hawkins, K., Hayes, C.R., Hermes, J.J., Hernández-García, L., Hogg, D.W., Holtzman, J.A., Ibarra-Medel, H.J., Ji, A., Jofre, P., Johnson, J.A., Jones, A.M., Kinemuchi, K., Kluge, M., Koekemoer, A., Kollmeier, J.A., Kounkel, M., Krishnarao, D., Krumpe, M., Lacerna, I., Lago, P.J.A., Laporte, C., Liu, C., Liu, A., Liu, X., Lopes, A.R., Macktoobian, M., Majewski, S.R., Malanushenko, V., Maoz, D., Masseron, T., Masters, K.L., Matijevic, G., McBride, A., Medan, I., Merloni, A., Morrison, S., Myers, N., Mészáros, S., Negrete, C.A., Nidever, D.L., Nitschelm, C., Oravetz, D., Oravetz, A., Pan, K., Peng, Y., Pinsonneault, M.H., Pogge, R., Qiu, D., Ramirez, S.V., Rix, H.-W., Fernández Rosso, D., Runnoe, J., Salvato, M., Sanchez, S.F., Santana, F.A., Saydjari, A., Sayres, C., Schlaufman, K.C., Schneider, D.P., Schwöpe, A., Serna, J., Shen, Y., Sobek, J., Song, Y.-Y., Souto, D., Spoo, T., Stassun, K.G., Steinmetz, M., Straumit, I., Stringfellow, G., Sánchez-Gallego, J., Taghizadeh-Popp, M., Tayar, J., Thakar, A., Tissera, P.B., Tkachenko, A., Hernandez Toledo, H., Trakhtenbrot, B., Fernández-Trincado, J.G., Troup, N., Trump, J.R., Tuttle, S., Ulloa, N., Vazquez-Mata, J.A., Vera Alfaro, P., Villanova, S., Wachter, S., Weijmans, A.-M., Wheeler, A., Wilson, J., Wojno, L., Wolf, J., Xue, X.-X., Ybarra, J.E., Zari, E., Zasowski, G., 2023. The Eighteenth Data Release of the Sloan Digital Sky Surveys: Targeting and First spectra from SDSS-V. *Astrophys. J. Suppl.* 267 (2), 44. <https://doi.org/10.3847/1538-4365/acda98>.
- Backhaus, B.E., Cleri, N.J., Trump, J.R., Kirkpatrick, A., Simons, R.C., Haro, P.A., Bagley, M.B., Brooks, M., Calabrò, A., Davis, K., Dickinson, M., Finkelstein, S.L., Hirschmann, M., Kartaltepe, J.S., Koekemoer, A.M., Llerena, M., Pacucci, F., Pirzkal, N., Papovich, C., Wilkins, S.M., 2025. Emission-Line Diagnostics at  $z > 4$ : [O III]  $\lambda 4363/\text{H}\gamma$ . preprint. <https://doi.org/10.48550/arXiv.2502.03519>.
- Baldwin, J.A., Phillips, M.M., Terlevich, R., 1981. Classification parameters for the emission-line spectra of extragalactic objects. *Publ. Astron. Soc. Pac.* 93, 5-19. <https://doi.org/10.1086/130766>.
- Balogh, M.L., Morris, S.L., Yee, H.K.C., Carlberg, R.G., Ellingson, E., 1999. Differential Galaxy Evolution in Cluster and Field Galaxies at  $z \sim 0.3$ . *Astrophys. J.* 527 (1), 54-79. <https://doi.org/10.1086/308056>.
- Barkhouse, W.A., Yee, H.K.C., López-Cruz, O., 2007. The Luminosity Function of Low-Redshift Abell Galaxy Clusters. *Astrophys. J.* 671 (2), 1471-1496. <https://doi.org/10.1086/523257>.
- Barkhouse, W.A., Yee, H.K.C., López-Cruz, O., 2009. The Galaxy Population of Low-redshift Abell Clusters. *Astrophys. J.* 703 (2), 2024-2032. <https://doi.org/10.1088/0004-637X/703/2/2024>.
- Barkhouse, W.A., Kashur, L.M., Akter, M., Kalawila, S.P., Gamage, G.L., López-Cruz, O., 2025. Properties of cluster red-sequence spiral galaxies. preprint. <https://arxiv.org/abs/2508.06896>.

- Bell, E.F., Kennicutt, Jr., R.C., 2001, A Comparison of Ultraviolet Imaging Telescope Far-Ultraviolet and H $\alpha$  Star Formation Rates. *Astrophys. J.* 548 (2), 681-693. <https://doi.org/10.1086/319025>.
- Bell, E.F., Wolf, C., Meisenheimer, K., Rix, H.-W., Borch, A., Dye, S., Kleinheinrich, M., Wisotzki, L., McIntosh, D.H., 2004. Nearly 5000 Distant Early-Type Galaxies in COMBO-17: A Red Sequence and Its Evolution since  $z \sim 1$ . *Astrophys. J.* 608 (2), 752-767. <https://doi.org/10.1086/420778>.
- Birchall, K.L., Watson, M.G., Aird, J., 2020. X-ray detected AGN in SDSS dwarf galaxies. *Mon. Notices RAS* 492 (2), 2268-2284. <https://doi.org/10.1093/mnras/staa040>.
- Birchall, K.L., Watson, M.G., Aird, J., Starling, R.L.C., 2022. The incidence of X-ray selected AGN in nearby galaxies. *Mon. Notices RAS* 510 (3), 4556-4572. <https://doi.org/10.1093/mnras/stab3573>.
- Bower, R.G., Benson, A.J., Malbon, R., Helly, J.C., Frenk, C.S., Baugh, C.M., Cole, S., Lacey, C.G., 2006. Breaking the hierarchy of galaxy formation. *Mon. Notices RAS* 370 (2), 645-655. <https://doi.org/10.1111/j.1365-2966.2006.10519.x>.
- Brandt, W.N., Alexander, D.M., 2015. Cosmic X-ray surveys of distant active galaxies. The demographics, physics, and ecology of growing supermassive black holes. *Astron. Astrophys. Rev.* 23, 1. <https://doi.org/10.1007/s00159-014-0081-z>.
- Brightman, M., Nandra, K., 2011. An XMM-Newton spectral survey of 12  $\mu\text{m}$  selected galaxies - I. X-ray data. *Mon. Notices RAS* 413 (2), 1206-1235. <https://doi.org/10.1111/j.1365-2966.2011.18207.x>.
- Brinchmann, J., Charlot, S., White, S.D.M., Tremonti, C., Kauffmann, G., Heckman, T., Brinkmann, J., 2004. The physical properties of star-forming galaxies in the low-redshift Universe. *Mon. Notices RAS* 351 (4), 1151-1179. <https://doi.org/10.1111/j.1365-2966.2004.07881.x>.
- Castelló-Mor, N., Barcons, X., Ballo, L., Carrera, F.J., Ward, M.J., Jin, C., 2012. The X-ray luminous galaxies optically classified as star forming are mostly narrow line Seyfert 1 s. *Astron. Astrophys.* 544, A48. <https://doi.org/10.1051/0004-6361/201118301>.
- Cheng, P., Chen, X., Liao, G., Gu, Y., Zheng, Q., Zhang, X., 2025. An improved Seyfert-low ionization nuclear emission-line region classification line in the [N II] BPT diagram. *Astron. Astrophys.* 699, A189. <https://doi.org/10.1051/0004-6361/202554434>.
- Chilingarian, I.V., Melchior, A.-L., Zolotukhin, I.Y., 2010. Analytical approximations of K-corrections in optical and near-infrared bands. *Mon. Notices RAS* 405 (3), 1409-1420. <https://doi.org/10.1111/j.1365-2966.2010.16506.x>.
- Chilingarian, I.V., Zolotukhin, I.Y., 2012. A universal ultraviolet-optical colour-colour-magnitude relation of galaxies. *Mon. Notices RAS* 419 (2), 1727-1739.

- Cid Fernandes, R., Stasińska, G., Schlickmann, M.S., Mateus, A., Vale Asari, N., Schoenell, W., Sodr , Jr, L., 2010. Alternative diagnostic diagrams and the ‘forgotten’ population of weak line galaxies in the SDSS. *Mon. Notices RAS* 403 (2), 1036-1053. <https://doi.org/10.1111/j.1365-2966.2009.16185.x>.
- Cid Fernandes, R., Stasińska, G., Mateus, A., Vale Asari, N., 2011. A comprehensive classification of galaxies in the Sloan Digital Sky Survey: how to tell true from fake AGN?. *Mon. Notices RAS* 413 (3), 1687-1699. <https://doi.org/10.1111/j.1365-2966.2011.18244.x>.
- Cresci, G., Maiolino, R., 2018. Observing positive and negative AGN feedback. *Nat. Astron* 2, 179-180. <https://doi.org/10.1038/s41550-018-0404-5>.
- Dhiwar, S., Saha, K., Dekel, A., Paswan, A., Pandey, D., Cortesi, A., Pandge, M., 2023. Witnessing the star formation quenching in L\* ellipticals. *Mon. Notices RAS* 518 (4), 4943-4960. <https://doi.org/10.1093/mnras/stac3369>.
- D az-Garc a, S., Moyano, F.D., Comer n, S., Knapen, J.H., Salo, H., Bouquin, A.Y.K., 2020. Distribution of star formation in galactic bars as seen with H $\alpha$  and stacked GALEX UV imaging. *Astron. Astrophys.* 644, A38. <https://doi.org/10.1051/0004-6361/202039162>.
- Dopita, M.A., Kewley, L.J., Heisler, C.A., Sutherland, R.S., 2000. A Theoretical Recalibration of the Extragalactic HII Region Sequence. *Astrophys. J.* 542 (1), 224-234. <https://doi.org/10.1086/309538>.
- Dubois, Y., Peirani, S., Pichon, C., Devriendt, J., Gavazzi, R., Welker, C., Volonteri, M., 2016. The HORIZON-AGN simulation: morphological diversity of galaxies promoted by AGN feedback. *Mon. Notices RAS* 463 (4), 3948-3964. <https://doi.org/10.1093/mnras/stw2265>.
- Evans, I.N., Evans, J.D., Mart nez-Galarza, J.R., Miller, J.B., Primini, F.A., Azadi, M., Burke, D.J., Civano, F.M., D’Abrusco, R., Fabbiano, G., Graessle, D.E., Grier, J.D., Houck, J.C., Lauer, J., McCollough, M.L., Nowak, M.A., Plummer, D.A., Rots, A.H., Siemiginowska, A., Tibbetts, M.S., 2024. The Chandra Source Catalog Release 2 Series. *Astrophys. J. Suppl. Ser.* 274 (2), 22. <https://doi.org/10.3847/1538-4365/ad6319>.
- Fabbiano, G., 1989. X-rays from normal galaxies. *Ann. Rev. Astron. Astrophys.* 27, 87-138. <https://doi.org/10.1146/annurev.aa.27.090189.000511>.
- Faber, S.M., Willmer, C.N.A., Wolf, C., Koo, D.C., Weiner, B.J., Newman, J.A., Im, M., Coil, A.L., Conroy, C., Cooper, M.C., Davis, M., Finkbeiner, D.P., Gerke, B.F., Gebhardt, K., Groth, E.J., Guhathakurta, P., Harker, J., Kaiser, N., Kassin, S., Kleinheinrich, M., Konidaris, N.P., Kron, R.G., Lin, L., Luppino, G., Madgwick, D.S., Meisenheimer, K., Noeske, K.G., Phillips, A.C., Sarajedini, V.L., Schiavon, R.P., Simard, L., Szalay, A.S., Vogt, N.P., Yan, R., 2007. Galaxy Luminosity Functions to  $z \sim 1$  from DEEP2 and COMBO-17: Implications for Red Galaxy Formation. *Astrophys. J.* 665 (1), 265-294. <https://doi.org/10.1086/519294>.

- Fabian, A.C., 2012. Observational Evidence of Active Galactic Nuclei Feedback. *Ann. Rev. Astron. Astrophys.* 50, 455-489. <https://doi.org/10.1146/annurev-astro-081811-125521>.
- Farage, C.L., McGregor, P.J., Dopita, M.A., Bocknell, G.V., 2010. Optical IFU Observations of the Brightest Cluster Galaxy NGC 4696: The Case for a Minor Merger and Shock-Excited Filaments. *Astrophys. J.* 724 (1), 267. <https://doi.org/10.1088/0004-637X/724/1/267>.
- Fasano, G., Marmo, C., Varela, J., D’Onofrio, M., Poggianti, B.M., Moles, M., Pignatelli, E., Bettoni, D., Kjærgaard, P., Rizzi, L., Couch, W.J., Dressler, A., 2006. WINGS: a WIde-field Nearby Galaxy-cluster Survey. I. Optical imaging. *Astron. Astrophys.* 445 (3), 805-817. <https://doi.org/10.1051/0004-6361:20053816>.
- Ferland, G.J., Netzer, H., 1983. Are there any shock-heated galaxies? *Astrophys. J.* 264, 105-113. <https://doi.org/10.1086/160577>.
- Halpern, J.P., Steiner, J.E., 1983. Low-ionization active galactic nuclei: X-ray or shock heated? *Astrophys. J.* 269, L37-L41. <https://doi.org/10.1086/184051>.
- Harrison, C.M., Alexander, D.M., Mullaney, J.R., Swinbank, A.M., 2014. Kiloparsec-scale outflows are prevalent among luminous AGN: outflows and feedback in the context of the overall AGN population. *Mon. Notices RAS* 441 (4), 3306-3347. <https://doi.org/10.1093/mnras/stu515>.
- Heckman, T.M., 1980. An Optical and Radio Survey of the Nuclei of Bright Galaxies - Activity in Normal Galactic Nuclei. *Astron. Astrophys.* 87, 152.
- Hickox, R.C., Jones, C., Forman, W.R., Murray, S.S., Kochanek, C.S., Eisenstein, D., Jannuzi, B.T., Dey, A., Brown, M.J.I., Stern, D., Eisenhardt, P.R., Gorjian, V., Brodwin, M., Narayan, R., Cool, R.J., Kenter, A., Caldwell, N., Anderson, M.E., 2009. Host Galaxies, Clustering, Eddington Ratios, and Evolution of Radio, X-ray, and Infrared-Selected AGNs. *Astrophys. J.* 696 (1), 891-919. <https://doi.org/10.1088/0004-637X/696/1/891>.
- Hickox, R.C., Alexander, D.M., 2018. Obscured Active Galactic Nuclei. *Ann. Rev. Astron. Astrophys.* 56, 625-671. <https://doi.org/10.1146/annurev-astro-081817-051803>.
- Ho, L.C., Filippenko, A.V., Sargent, W.L.W., 2003. A Search for “Dwarf” Seyfert Nuclei. VI. Properties of Emission-Line Nuclei in Nearby Galaxies. *Astrophys. J.* 583 (1), 159-177. <https://doi.org/10.1086/345354>.
- Ho, L.C., 2008. Nuclear Activity in Nearby Galaxies. *Ann. Rev. Astron. Astrophys.* 46, 475-539. <https://doi.org/10.1146/annurev.astro.45.051806.110546>.
- Ishibashi, W., Fabian, A.C., 2012. Active galactic nucleus feedback and triggering of star formation in galaxies. *Mon. Notices RAS* 427 (4), 2998-3005. <https://doi.org/10.1111/j.1365-2966.2012.22074.x>.

- Jarrett, T.H., Cohen, M., Masci, F., Wright, E., Stern, D., Benford, D., Blain, A., Carey, S., Cutri, R.M., Eisenhardt, P., Lonsdale, C., Mainzer, A., Marsh, K., Padgett, D., Petty, S., Ressler, M., Skrutskie, M., Stanford, S., Surace, J., Tsai, C.W., Wheelock, S., Yan, D.L., 2011. The Spitzer-WISE Survey of the Ecliptic Poles. *Astrophys. J.* 735 (2), 112. <https://doi.org/10.1088/0004-637X/735/2/112>.
- Jarrett, T.H., Masci, F., Tsai, C.W., Petty, S., Cluver, M.E., Assef, R.J., Benford, D., Blain, A., Bridge, C., Donoso, E., Eisenhardt, P., Koribalski, B., Lake, S., Neill, J.D., Seibert, M., Sheth, K., Stanford, S., Wright, E., 2013. Extending the Nearby Galaxy Heritage with WISE: First Results from the WISE Enhanced Resolution Galaxy Atlas. *Astron. J.* 145 (1), 6. <https://doi.org/10.1088/0004-6256/145/1/6>.
- Kauffmann, G., Heckman, T.M., Tremonti, C., Brinchmann, J., Charlot, S., White, S.D.M., Ridgway, S.E., Brinkmann, J., Fukugita, M., Hall, P.B., Ivezić, Ž, Richards, G.T., Schneider, D.P., 2003. The host galaxies of active galactic nuclei. *Mon. Notices RAS* 346 (4), 1055-1077. <https://doi.org/10.1111/j.1365-2966.2003.07154.x>.
- Kewley, L.J., Heisler, C.A., Dopita, M.A., Lumsden, S., 2001. Optical Classification of Southern Warm Infrared Galaxies. *Astrophys. J. Suppl. Ser.* 132 (1), 37-71. <https://doi.org/10.1086/318944>.
- Kewley, L.J., Dopita, M.A., Sutherland, R.S., Heisler, C.A., Trevena, J., 2001. Theoretical Modeling of Starburst Galaxies. *Astrophys. J.* 556 (1), 121-140. <https://doi.org/10.1086/321545>.
- Kewley, L.J., Groves, B., Kauffmann, G., Heckman, T., 2006. The host galaxies and classification of active galactic nuclei. *Mon. Notices RAS* 372 (3), 961-976. <https://doi.org/10.1111/j.1365-2966.2006.10859.x>.
- Kewley, L.J., Nicholls, D.C., Sutherland, R., Rigby, J.R., Acharya, A., Dopita, M.A., Bayliss, M.B., 2019. Theoretical ISM Pressure and Electron Density Diagnostics for Local and High-Redshift Galaxies. *Astrophys. J.* 880 (1), 16. <https://doi.org/10.3847/1538-4357/ab16ed>.
- Kormendy, J., Ho, L.C., 2013. Coevolution (Or Not) of Supermassive Black Holes and Host Galaxies. *Ann. Rev. Astron. Astrophys.* 51, 511-653. <https://doi.org/10.1146/annurev-astro-082708-101811>.
- Lacerda, E.A.D., Sánchez, S.F., Cid Fernandes, R., López-Cobá, C., Espinosa-Ponce, C., Galbany, L., 2020. Galaxies hosting an active galactic nucleus: a view from the CALIFA survey. *Mon. Notices RAS* 492 (3), 3073-3090. <https://doi.org/10.1093/mnras/staa008>.
- Lehmer, B.D., Basu-Zych, A.R., Mineo, S., Brandt, W.N., Eufrazio, R.T., Fragos, T., Hornschemeier, A.E., Luo, B., Xue, Y.Q., Bauer, F.E., Gilfanov, M., Ranalli, P., Schneider, D.P., Shemmer, O., Tozzi, P., Trump, J.R., Vignali, C., Wang, J.-X., Yukita, M., Zezas, A., 2016. The Evolution of Normal Galaxy X-ray Emission through Cosmic History: Constraints from the 6 MS Chandra Deep Field-South. *Astrophys. J.* 825 (1), 24. <https://doi.org/10.3847/0004-637X/825/1/7>.

- Lesser, J.N., 2022. Origin Of Red Sequence Barred Spiral Galaxies. M.S. Thesis. The University of North Dakota. <https://commons.und.edu/theses/4353>.
- Łokas, E.L., 2022. The origin and properties of red spirals: Insights from cosmological simulations. *Astron. Astrophys.* 667, A27. <https://doi.org/10.1051/0004-6361/202244284>.
- López-Cruz, O., Barkhouse, W.A., Yee, H.K.C., 2004. The Color-Magnitude Effect in Early-Type Cluster Galaxies. *Astrophys. J.* 614 (2), 679-691. <https://doi.org/10.1086/423664>.
- Luo, R., Woo, J.-H., Karouzos, M., Bae, H.-J., Shin, J., McConnell, N., Shih, H.-Y., Kim, Y.J., Park, S., 2021. Unraveling the Complex Structure of AGN-driven Outflows. V. Integral-field Spectroscopy of 40 Moderate-luminosity Type-2 AGNs. *Astrophys. J.* 908 (2), 221. <https://doi.org/10.3847/1538-4357/abd5ac>.
- Mahajan, S., Drinkwater, M.J., Driver, S., Hopkins, A.M., Graham, A.W., Brough, S., Brown, M.J.I., Holwerda, B.W., Owers, M.S., Pimbblet, K.A., 2018. Galaxy And Mass Assembly (GAMA): blue spheroids within 87 Mpc. *Mon. Notices RAS* 475 (1), 788-799. <https://doi.org/10.1093/mnras/stx3202>.
- Martini, P., Kelson, D.D., Mulchaey, J.S., Trager, S.C., 2002. An Unexpectedly High Fraction of Active Galactic Nuclei in Red Cluster Galaxies. *Astrophys. J.* 576 (2), L109. <https://doi.org/10.1086/343729>.
- Masters, K.L., Mosleh, M., Romer, A.K., Nichol, R.C., Bamford, S.P., Schawinski, K., Lintott, C.J., Andreescu, D., Campbell, H.C., Crowcroft, B., Doyle, I., Edmondson, E.M., Murray, P., Raddick, M.J., Slosar, A., Szalay, A.S., Vandenberg, J., 2010. Galaxy Zoo: passive red spirals. *Mon. Notices RAS* 405 (2), 783-799. <https://doi.org/10.1111/j.1365-2966.2010.16503.x>.
- Mazzolari, G., Übler, H., Maiolino, R., Ji, X., Nakajima, K., Feltre, A., Scholtz, J., D'Eugenio, F., Curti, M., Mignoli, M., Marconi, A., 2024. New AGN diagnostic diagrams based on the [O III] $\lambda$ 4363 auroral line. *Astron. Astrophys.* 691, A345. <https://doi.org/10.1051/0004-6361/202450407>.
- Mazzolari, G., Scholtz, J., Maiolino, R., Gilli, R., Traina, A., López, I.E., Übler, H., Trefoloni, B., D'Eugenio, F., Ji, X., Mignoli, M., Vito, F., Vignali, C., Brusa, M., 2025. Narrow line AGN selection in CEERS: spectroscopic selection, physical properties, X-ray and radio analysis. *Astron. Astrophys.* 700, A12. <https://doi.org/10.1051/0004-6361/202451860>.
- Moran, E.C., Lehnert, M.D., Helfand, D.J., 1999. X-Rays from NGC 3256: High-Energy Emission in Starburst Galaxies and Their Contribution to the Cosmic X-Ray Background. *Astrophys. J.* 526 (2), 649-664. <https://doi.org/10.1086/308008>.
- Moretti, A., Poggianti, B.M., Fasano, G., Bettoni, D., D'Onofrio, M., Fritz, J., Cava, A., Varela, J., Vulcani, B., Gullieuszik, M., Couch, W.J., Omizzolo, A., Valentiniuzzi, T., Dressler, A., Moles, M., Kjærgaard, P., Smareglia, R., Molinaro, M., 2014.

- WINGS Data Release: a database of galaxies in nearby clusters. *Astron. Astrophys.* 564, A138. <https://doi.org/10.1051/0004-6361/201323098>.
- Morganti, R., 2017. The Many Routes to AGN Feedback. *Front. Astron. Space Sci.* 4, 42. <https://doi.org/10.3389/fspas.2017.00042>.
- Noguchi, M., 1996. Barred Galaxies: Intrinsic or Extrinsic? *Astrophys. J.* 469, 605. <https://doi.org/10.1086/177809>.
- Padovani, P., Alexander, D.M., Assef, R.J., De Marco, B., Giommi, P., Hickox, R.C., Richards, G.T., Smolčić, V., Hatziminaoglou, E., Mainieri, V., Salvato, M., 2017. Active galactic nuclei: what's in a name?. *Astron. Astrophys. Rev.* 25 (1), 2. <https://doi.org/10.1007/s00159-017-0102-9>.
- Peterson, B.M., 2013. Measuring the Masses of Supermassive Black Holes. *Space Science Reviews*. Falanga, M., Belloni, T., Casella, P., Gilfanov, M., Jonker, P., King, A. (eds) *The Physics of Accretion onto Black Holes*. Space Sciences Series of ISSI, vol 49. Springer, New York, NY. [https://doi.org/10.1007/978-1-4939-2227-7\\_13](https://doi.org/10.1007/978-1-4939-2227-7_13).
- Pierce, C.M., Lotz, J.M., Laird, E.S., Lin, L., Nandra, K., Primack, J.R., Faber, S.M., Barmby, P., Park, S.Q., Willner, S.P., Gwyn, S., Koo, D.C., Coil, A.L., Cooper, M.C., Georgakakis, A., Koekemoer, A.M., Noeske, K.G., Weiner, B.J., Willmer, C.N.A., 2007. AEGIS: Host Galaxy Morphologies of X-ray-selected and Infrared-selected Active Galactic Nuclei at  $0.2 \leq z < 1.2$ . *Astrophys. J.* 660 (1), L19-L22. <https://doi.org/10.1086/517922>.
- Pons, E., Watson, M.G., 2014. A new sample of X-ray-selected narrow emission-line galaxies. I. The nature of optically elusive AGN. *Astron. Astrophys.* 568, A108. <https://doi.org/10.1051/0004-6361/201423866>.
- Pons, E., 2016. Investigations of AGN populations through X-ray and optical surveys. Ph.D. thesis, University of Leicester. <https://hdl.handle.net/2381/38037>.
- Pović, M., Sánchez-Portal, M., Pérez García, A.M., Bongiovanni, A., Cepa, J., Huertas-Company, M., Lara-López, M.A., Fernández Lorenzo, M., Ederoclite, A., Alfaro, E., Castañeda, H., Gallego, J., González-Serrano, J.I., González, J.J., 2012. AGN–host galaxy connection: morphology and colours of X-ray selected AGN at  $z \leq 2$ . *Astron. Astrophys.* 541, A118. <https://doi.org/10.1051/0004-6361/201117314>.
- Raouf, M., Purabbas, M.H., Hesar, F.F., 2024. Impact of Active Galactic Nuclei Feedback on the Dynamics of Gas: A Review across Diverse Environments. *Galaxies*, 12 (2), 16. <https://doi.org/10.3390/galaxies12020016>.
- Rich, J.A., Kewley, J., Dopita, M.A., 2011. Galaxy-Wide Shocks in Late-Merger Stage Luminous Infrared Galaxies, 734 (2), 87. <https://doi.org/10.1088/0004-637X/734/2/87>.
- Rubinur, K., 2024. AGN Feedback Signatures in UV Emission. *Galaxies*, 12 (2), 15. <https://doi.org/10.3390/galaxies12020015>.

- Rude, C.M., Sultanova, M.R., Ipita kaduwa Gamage, G.L., Barkhouse, W.A., Kalawila Vithanage, S.P., 2020. Star formation in low-redshift cluster dwarf galaxies. *Mon. Notices RAS* 493 (4), 5625-5635. <https://doi.org/10.1093/mnras/staa697>.
- Salim, S., 2014. Green Valley Galaxies. *Serb. Astron. J.* 189, 1-4. <https://doi.org/10.2298/SAJ1489001S>.
- Schawinski, K., Thomas, D., Sarzi, M., Maraston, C., Kaviraj, S., Joo, S.-J., Yi, S.K., Silk, J., 2007. Observational evidence for AGN feedback in early-type galaxies. *Mon. Notices RAS* 382 (4), 1415-1431. <https://doi.org/10.1111/j.1365-2966.2007.12487.x>.
- Schlafly, E.F., Finkbeiner, D.P., 2011. Measuring Reddening with Sloan Digital Sky Survey Stellar Spectra and Recalibrating SFD. *Astrophys. J.* 737 (2), 103. <https://doi.org/10.1088/0004-637X/737/2/103>.
- Scholtz, J., Maiolino, R., D'Eugenio, F., Curtis-Lake, E., Carniani, S., Charlot, S., Curti, M., Silcock, M.S., Arribas, S., Baker, W., Bhatawdekar, R., Boyett, K., Bunker, A.J., Chevallard, J., Circosta, C., Eisenstein, D.J., Hainline, K., Hausen, R., Ji, X., Ji, Z., Johnson, B.D., Kumari, N., Looser, T.J., Lyu, J., Maseda, M.V., Parlanti, E., Perna, M., Rieke, M., Robertson, B., Del Pino, B.R., Sun, F., Tacchella, S., Übler, H., Venturi, G., Williams, C.C., Willmer, C.N.A., Willott, C., Witstok, J., 2025. JADES: A large population of obscured, narrow-line active galactic nuclei at high redshift. *Astron. Astrophys.* 697, A175. <https://doi.org/10.1051/0004-6361/202348804>.
- Shakura, N.I., Sunyaev, R.A., 1973. Black holes in binary systems. Observational appearance. *Astron. Astrophys.* 24, 337-355.
- Shang, Z., Brotherton, M.S., Wills, B.J., Wills, D., Cales, S.L., Dale, D.A., Green, R.F., Runnoe, J.C., Nemmen, R.S., Gallagher, S.C., Ganguly, R., Hines, D.C., Kelly, B.J., Kriss, G.A., Li, J., Tang, B., Xie, Y., 2011. The Next Generation Atlas of Quasar Spectral Energy Distributions from Radio to X-rays. *Astrophys. J. Suppl.* 196 (1), 2. <https://doi.org/10.1088/0067-0049/196/1/2>.
- Silk, J., 2013. Unleashing Positive Feedback: Linking the Rates of Star Formation, Supermassive Black Hole Accretion, and Outflows in Distant Galaxies. *Astrophys. J.* 772 (2), 112. <https://doi.org/10.1088/0004-637X/772/2/112>.
- Silverman, J.D., Green, P.J., Barkhouse, W.A., Kim, D.-W., Kim, M., Wilkes, B.J., Cameron, R.A., Hasinger, G., Jannuzi, B.T., Smith, M.G., Smith, P.S., Tananbaum, H., 2008. The Luminosity Function of X-ray-selected Active Galactic Nuclei: Evolution of Supermassive Black Holes at High Redshift. *Astrophys. J.* 679 (1), 118-139. <https://doi.org/10.1086/529572>.
- Singh, R., van de Ven, G., Jahnke, K., Lyubenova, M., Falcón-Barroso, J., Alves, J., Cid Fernandes, R., Galbany, L., García-Benito, R., Husemann, B., Kennicutt, R.C., Marino, R.A., Márquez, I., Masegosa, J., Mast, D., Pasquali, A., Sánchez, S.F., Walcher, J., Wild, V., Wisotzki, L., Ziegler, B., 2013. The nature of LINER galaxies:

- Ubiquitous hot old stars and rare accreting black holes. *Astron. Astrophys.* 558, A43. <https://doi.org/10.1051/0004-6361/201322062>.
- Stasińska, G., Cid Fernandes, R., Mateus, A., Sodré, L., Asari, N.V., 2006. Semi-empirical analysis of Sloan Digital Sky Survey galaxies - III. How to distinguish AGN hosts. *Mon. Notices RAS* 371 (2), 972-982. <https://doi.org/10.1111/j.1365-2966.2006.10732.x>.
- Stemo, A., Comerford, J.M., Barrows, R.S., Stern, D., Assef, R.J., Griffith, R.L., 2020. A Catalog of AGN Host Galaxies Observed with HST/ACS: Correlations between Star Formation and AGN Activity. *Astrophys. J.* 888 (2), 78. <https://doi.org/10.3847/1538-4357/ab5f66>.
- Terlevich, R., Melnick, J., 1985. Warmers: the missing link between Starburst and Seyfert galaxies. *Mon. Notices RAS* 213, 841-856. <https://doi.org/10.1093/mnras/213.4.841>.
- Tremonti, C.A., Heckman, T.M., Kauffmann, G., Brinchmann, J., Charlot, S., White, S.D.M., Seibert, M., Peng, E.W., Schlegel, D.J., Uomoto, A., Fukugita, M., Brinkmann, J., 2004. The Origin of the Mass-Metallicity Relation: Insights from 53,000 Star-forming Galaxies in the Sloan Digital Sky Survey. *Astrophys. J.* 613, 898-913. <https://doi.org/10.1086/423264>.
- Trouille, L., Barger, A., 2010. The OPTX Project: Comparing the Optical and X-Ray Spectral Properties of Active Galactic Nuclei. *Co-Evolution of Central Black Holes and Galaxies, Proceedings of the International Astronomical Union, IAU Symposium*, 267, 142-142. <https://doi.org/10.1017/S1743921310006034>.
- Trouille, L., Barger, A.J., Tremonti, C., 2011. The OPTX Project. V. Identifying Distant Active Galactic Nuclei. *Astrophys. J.* 742 (1), 46. <https://doi.org/10.1088/0004-637X/742/1/46>.
- Valentinuzzi, T., Poggianti, B.M., Fasano, G., D'Onofrio, M., Moretti, A., Ramella, M., Biviano, A., Fritz, J., Varela, J., Bettoni, D., Vulcani, B., Moles, M., Couch, W.J., Dressler, A., Kjørgaard, P., Omizzolo, A., Cava, A., 2011. The red-sequence of 72 WINGS local galaxy clusters. *Astron. Astrophys.* 536, A34. <https://doi.org/10.1051/0004-6361/201117522>.
- van den Bergh, S., 1998, *Galaxy Morphology and Classification* (Cambridge: Cambridge Univ. Press)
- Varela, J., D'Onofrio, M., Marmo, C., Fasano, G., Bettoni, D., Cava, A., Couch, W.J., Dressler, A., Kjørgaard, P., Moles, M., Pignatelli, E., Poggianti, B.M., Valentinuzzi, T., 2009. WINGS: A Wide-field Nearby Galaxy-cluster Survey. II. Deep optical photometry of 77 nearby clusters. *Astron. Astrophys.* 497 (3), 667-676. <https://doi.org/10.1051/0004-6361/200809876>.
- Veilleux, S., Osterbrock, D.E., 1987. Spectral Classification of Emission-Line Galaxies. *Astrophys. J. Suppl. Ser.* 63, 295. <https://doi.org/10.1086/191166>.

- Venturi, G., Treister, E., Finlez, C., D'Ago, G., Bauer, F., Harrison, C.M., Ramos Almeida, C., Revalski, M., Ricci, F., Sartori, L.F., Girdhar, A., Keel, W.C., Tubín, D., 2023. Complex AGN feedback in the Teacup galaxy. A powerful ionised galactic outflow, jet-ISM interaction, and evidence for AGN-triggered star formation in a giant bubble. *Astron. Astrophys.* 678, A127. <https://doi.org/10.1051/0004-6361/202347375>.
- Wagner, A.Y., Bicknell, G.V., Umemura, M., Sutherland, R.S., Silk, J., 2016. Galaxy-scale AGN feedback – theory. *Astron. Nachr.* 337, 167-174. <https://doi.org/10.1002/asna.201512287>.
- Wang, T., Elbaz, D., Alexander, D.M., Xue, Y.Q., Gabor, J.M., Juneau, S., Schreiber, C., Zheng, X.-Z., Wuyts, S., Shi, Y., Daddi, E., Shu, X.-W., Fang, G.-W., Huang, J.-S., Luo, B., Gu, Q.-S., 2017. AGN-host connection at  $0.5 < z < 2.5$ : A rapid evolution of AGN fraction in red galaxies during the last 10 Gyr. *Astron. Astrophys.* 601, A63. <https://doi.org/10.1051/0004-6361/201526645>.
- Wright, E.L., Eisenhardt, P.R.M., Mainzer, A.K., Ressler, M.E., Cutri, R.M., Jarrett, T., Kirkpatrick, J.D., Padgett, D., McMillan, R.S., Skrutskie, M., Stanford, S.A., Cohen, M., Walker, R.G., Mather, J.C., Leisawitz, D., Gautier, T.N., III, McLean, I., Benford, D., Lonsdale, C.J., Blain, A., Mendez, B., Irace, W.R., Duval, V., Liu, F., Royer, D., Heinrichsen, I., Howard, J., Shannon, M., Kendall, M., Walsh, A.L., Larsen, M., Cardon, J.G., Schick, S., Schwalm, M., Abid, M., Fabinsky, B., Naes, L., Tsai, C.-W., 2010. The Wide-field Infrared Survey Explorer (WISE): Mission Description and Initial On-orbit Performance. *Astron. J.* 140 (6), 1868-1881. <https://doi.org/10.1088/0004-6256/140/6/1868>.
- Yahil, A., Vidal, N.V., 1977. The Velocity Distribution of Galaxies in Clusters. *Astrophys. J.* 214, 347-350. <https://doi.org/10.1086/155257>.
- Yao, Z., Yuan, F., Ostriker, J.P., 2021. Active galactic nucleus feedback in an elliptical galaxy with the most updated AGN physics: Parameter explorations. *Mon. Notices RAS* 501 (1), 398-410. <https://doi.org/10.1093/mnras/staa3755>.
- York, D.G., Adelman, J., Anderson, J.E., Jr., Anderson, S.F., Annis, J., Bahcall, N.A., Bakken, J.A., Barkhouser, R., Bastian, S., Berman, E., Boroski, W.N., Bracker, S., Briegel, C., Briggs, J.W., Brinkmann, J., Brunner, R., Burles, S., Carey, L., Carr, M.A., Castander, F.J., Chen, B., Colestock, P.L., Connolly, A.J., Crocker, J.H., Csabai, I., Czarapata, P.C., Davis, J.E., Doi, M., Dombeck, T., Eisenstein, D., Ellman, N., Elms, B.R., Evans, M.L., Fan, X., Federwitz, G.R., Fiscelli, L., Friedman, S., Frieman, J.A., Fukugita, M., Gillespie, B., Gunn, J.E., Gurbani, V.K., de Haas, E., Haldeman, M., Harris, F.H., Hayes, J., Heckman, T.M., Hennessy, G.S., Hindsley, R.B., Holm, S., Holmgren, D.J., Huang, C.-H., Hull, C., Husby, D., Ichikawa, S.-I., Ichikawa, T., Ivezić, Ž., Kent, S., Kim, R.S.J., Kinney, E., Klaene, M., Kleinman, A.N., Kleinman, S., Knapp, G.R., Korienek, J., Kron, R.G., Kunszt, P.Z., Lamb, D.Q., Lee, B., Leger, R.F., Limmongkol, S., Lindenmeyer, C., Long, D.C., Loomis, C., Loveday, J., Lucinio, R., Lupton, R.H., MacKinnon, B., Mannery, E.J., Mantsch, P.M., Margon, B., McGehee, P., McKay, T.A., Meiksin, A., Merelli, A., Monet,

- D.G., Munn, J.A., Narayanan, V.K., Nash, T., Neilsen, E., Neswold, R., Newberg, H.J., Nichol, R.C., Nicinski, T., Nonino, M., Okada, N., Okamura, S., Ostriker, J.P., Owen, R., Pauls, A.G., Peoples, J., Peterson, R.L., Petravick, D., Pier, J.R., Pope, A., Pordes, R., Prosapio, A., Rechenmacher, R., Quinn, T.R., Richards, G.T., Richmond, M.W., Rivetta, C.H., Rockosi, C.M., Ruthmansdorfer, K., Sandford, D., Schlegel, D.J., Schneider, D.P., Sekiguchi, M., Sergey, G., Shimasaku, K., Siegmund, W.A., Smee, S., Smith, J.A., Snedden, S., Stone, R., Stoughton, C., Strauss, M.A., Stubbs, C., SubbaRao, M., Szalay, A.S., Szapudi, I., Szokoly, G.P., Thakar, A.R., Tremonti, C., Tucker, D.L., Uomoto, A., Vanden Berk, D., Vogeley, M.S., Waddell, P., Wang, S.-i., Watanabe, M., Weinberg, D.H., Yanny, B., Yasuda, N., 2000. The Sloan Digital Sky Survey: Technical Summary. *Astron. J.* 120 (3), 1579-1587. <https://doi.org/10.1086/301513>.
- Zezas, A. L., Georgantopoulos, I., Ward, M.J., 1998. ROSAT and ASCA observations of X-ray luminous starburst galaxies: NGC 3310 and 3690. *Mon. Notices RAS* 301 (4), 915-925. <https://doi.org/10.1046/j.1365-8711.1998.01993.x>.
- Zinn, P.-C., Middelberg, E., Norris, R.P., Dettmar, R.-J., 2013. Active Galactic Nucleus Feedback Works Both Ways. *Astrophys. J.* 774 (1), 66. <https://doi.org/10.1088/0004-637X/774/1/66>.

Table 1: Summary of galaxy classification using optical emission-line ratios.

Emission Line Ratio	No. of Galaxies	Star-Forming	AGN/Seyfert	LINERs
$\log ([\text{O III}]/\text{H}\beta)$ vs $\log ([\text{N II}]/\text{H}\alpha)$	Blue (102)	81 (79.4%)	19 (18.6%)	2 (2%)
$\log ([\text{O III}]/\text{H}\beta)$ vs $\log ([\text{S II}]/\text{H}\alpha)$	Blue (91)	85 (93.4%)	3 (3.3%)	3 (3.3%)
$\log ([\text{O III}]/\text{H}\beta)$ vs $\log ([\text{O I}]/\text{H}\alpha)$	Blue (31)	25 (80.6%)	4 (12.9%)	2 (6.4%)
$\log ([\text{O III}]/\text{H}\gamma)$ vs $\log ([\text{O III}]/[\text{O II}])$	Blue (10)	0* (0%)	10 (100%)	
$\log ([\text{O III}]/\text{H}\gamma)$ vs $\log ([\text{Ne III}]/[\text{O II}])$	Blue (9)	1 (11.1%)	7 (77.8%)	1* (11.1%)
$\log ([\text{O III}]/[\text{O II}])$ vs $\log ([\text{N II}]/\text{H}\alpha)$	Blue (97)	85 (87.6%)	8 (8.2%)	4 (4.1%)
$\log ([\text{O III}]/\text{H}\alpha)$ vs $\log ([\text{N II}]/\text{H}\alpha)$	Blue (95)	88 (92.6%)	7 (7.4%)	0 (0%)
	Red (71)	11 (15.5%)	46 (64.8%)	14 (19.7%)
	Red (54)	15 (27.8%)	3 (5.6%)	36 (66.7%)
	Red (42)	2 (4.8%)	5 (11.9%)	35 (83.3%)
	Red (68)	2* (2.9%)	66 (97.1%)	
	Red (56)	2 (3.6%)	37 (66.1%)	17* (30.3%)
	Red (75)	22 (29.3%)	24 (32%)	29 (38.7%)
	Red (62)	15 (24.2%)	37 (59.7%)	10 (16.1%)

\*Based on [Mazzolari et al. \(2024\)](#) “Star-forming or AGN/Seyfert” classification.

Table 2: Properties of galaxies that are located in the AGN section of the *WISE* diagram.

Cluster	RA (deg)	Dec (deg)	$L_x$ (erg s <sup>-1</sup> )	$\Delta L_x$ (erg s <sup>-1</sup> )	<i>WISE</i> Classification
A3158	55.4353981	-53.7059441	$1.469 \times 10^{43}$	$4.724 \times 10^{41}$	Blue (AGN)
A500	69.6615982	-22.0569439	$2.912 \times 10^{43}$	$3.143 \times 10^{41}$	Blue (AGN)
A655	126.456570	47.1745300	$5.056 \times 10^{43}$	$2.051 \times 10^{42}$	Blue (AGN)
A795	141.122570	14.3926220	$5.336 \times 10^{42}$	$1.431 \times 10^{42}$	Blue (SF)
A1291	173.268585	56.1747971	$1.312 \times 10^{42}$	$6.713 \times 10^{41}$	Blue (SF)
A1736	202.041656	-27.3318005	$9.950 \times 10^{42}$	$4.106 \times 10^{41}$	Red (AGN)
A1920	216.693880	55.2271420	Not detected	Not detected	Blue (AGN)
A2199	247.636030	39.3841500	$2.994 \times 10^{42}$	$6.199 \times 10^{40}$	Blue (AGN)

Table 3: K-S test result statistics of red and blue spiral galaxies using emission-line diagnostic diagrams.

Emission Line Ratio	D-Statistic	Probability
$\log ([\text{O III}]/\text{H}\beta)$ vs. $\log ([\text{N II}]/\text{H}\alpha)$	0.63	0.00
$\log ([\text{O III}]/\text{H}\beta)$ vs. $\log ([\text{S II}]/\text{H}\alpha)$	0.68	0.00
$\log ([\text{O III}]/\text{H}\beta)$ vs. $\log ([\text{O I}]/\text{H}\alpha)$	0.78	0.00
$\log ([\text{O III}]/\text{H}\gamma)$ vs. $\log ([\text{O III}]/[\text{O II}])$	0.31	0.40
$\log ([\text{O III}]/\text{H}\gamma)$ vs. $\log ([\text{Ne III}]/[\text{O II}])$	0.19	0.50
$\log ([\text{O III}]/[\text{O II}])$ vs. $\log ([\text{N II}]/\text{H}\alpha)$	0.43	0.00
$\log ([\text{O III}]/\text{H}\alpha)$ vs. $\log ([\text{N II}]/\text{H}\alpha)$	0.43	0.00

Table 4: Classification of blue spirals based on emission-line ratio diagrams.

$\log L_X$ ( $\text{erg s}^{-1}$ )	$\Delta L_X$ ( $\text{erg s}^{-1}$ )	[O III]/H $\beta$ vs [N II]/H $\alpha$	[O III]/H $\beta$ vs [S II]/H $\alpha$	[O III]/H $\beta$ vs [O I]/H $\alpha$	[O III]/H $\gamma$ vs [O III]/[O II]	[O III]/H $\gamma$ vs [Ne III]/[O II]	[O III]/[O II] vs [N II]/H $\alpha$	[O III]/H $\alpha$ vs [N II]/H $\alpha$	WHAN
$2.994 \times 10^{42}$	$6.199 \times 10^{40}$	AGN	AGN	AGN	None	None	AGN	AGN	Retired
$5.909 \times 10^{40}$	$3.668 \times 10^{40}$	SF	SF	None	None	None	LINERs	LINERs	Retired
$1.214 \times 10^{41}$	$1.644 \times 10^{40}$	AGN	AGN	AGN	None	None	AGN	AGN	Retired
$2.299 \times 10^{41}$	$1.428 \times 10^{40}$	SF	SF	None	None	None	None	SF	Retired
$1.152 \times 10^{41}$	$2.810 \times 10^{40}$	None	None	None	None	None	None	None	Retired
$5.056 \times 10^{43}$	$2.051 \times 10^{42}$	AGN	None	None	None	AGN/SF	None	LINERs	None
$5.336 \times 10^{42}$	$1.431 \times 10^{42}$	AGN	SF	None	None	None	LINERs	LINERs	Retired
$1.312 \times 10^{42}$	$6.713 \times 10^{41}$	AGN	AGN	AGN	None	None	SF	AGN	None
$3.402 \times 10^{40}$	$2.952 \times 10^{40}$	SF	SF	SF	None	None	SF	SF	Retired

Table 5: Classification of red spirals based on emission-line ratio diagrams.

$\log L_X$ ( $\text{erg s}^{-1}$ )	$\Delta L_X$ ( $\text{erg s}^{-1}$ )	[O III]/H $\beta$ vs [N II]/H $\alpha$	[O III]/H $\beta$ vs [S II]/H $\alpha$	[O III]/H $\beta$ vs [O I]/H $\alpha$	[O III]/H $\gamma$ vs [O III]/[O II]	[O III]/H $\gamma$ vs [Ne III]/[O II]	[O III]/[O II] vs [N II]/H $\alpha$	[O III]/H $\alpha$ vs [N II]/H $\alpha$	WHAN
$1.701 \times 10^{40}$	$1.243 \times 10^{40}$	None	None	None	AGN	SF/AGN	LINERs	LINERs	Passive
$1.635 \times 10^{40}$	$3.850 \times 10^{40}$	Comp	SF	None	None	None	None	None	Passive
$2.842 \times 10^{41}$	$9.958 \times 10^{39}$	None	None	None	AGN	None	LINERs	LINERs	Passive
$9.917 \times 10^{39}$	$4.749 \times 10^{39}$	None	None	None	AGN	SF/AGN	LINERs	LINERs	Passive
$8.226 \times 10^{39}$	$3.045 \times 10^{39}$	SF	SF	None	None	None	SF	SF	Retired
$7.022 \times 10^{40}$	$3.865 \times 10^{40}$	LINERs	None	None	AGN	AGN	AGN	None	None
$4.624 \times 10^{41}$	$3.078 \times 10^{40}$	None	None	None	AGN	SF/AGN	LINERs	LINERs	Passive
$9.511 \times 10^{40}$	$2.253 \times 10^{40}$	AGN/Comp	SF	None	AGN	None	AGN	SF	Retired

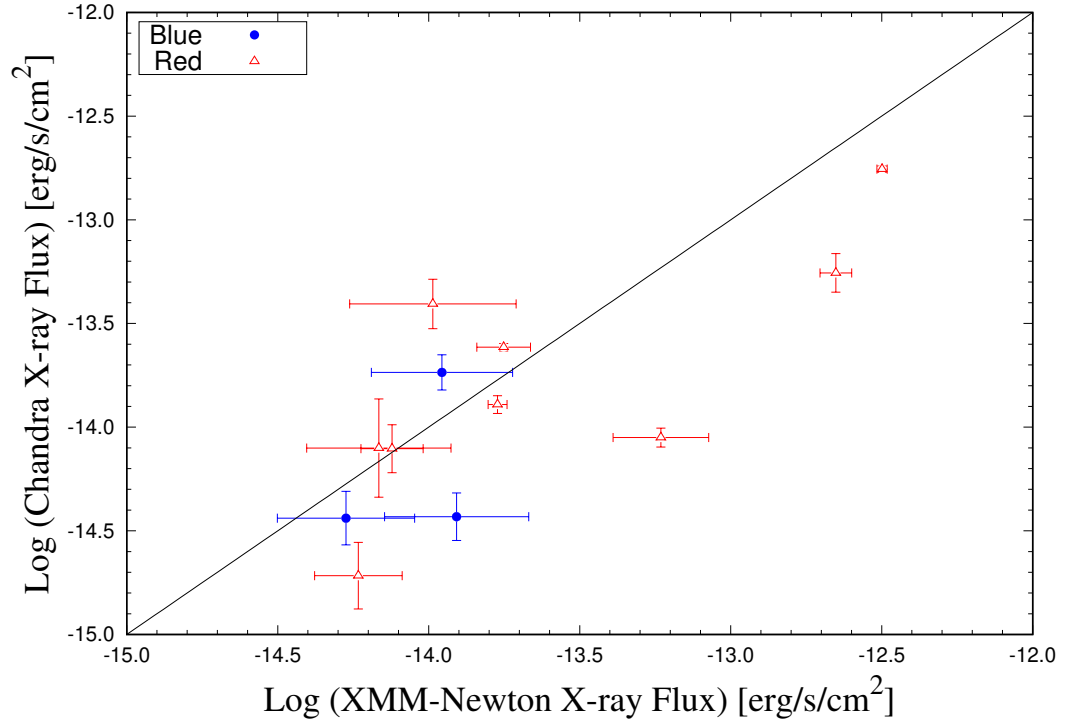


Figure A.1: Comparison between *XMM-Newton* and *Chandra* X-ray flux measurements for three blue spirals and nine red spiral galaxies that have measured fluxes from both telescopes. Two red spirals have flux measurements that disagree by  $> 3\sigma$ . The solid black line depicts equal flux measured by both telescopes.

### Appendix A. Comparison of X-ray flux measurements

In Figure A.1 we show the comparison of X-ray flux measured for three blue spirals and nine red spirals observed by both *Chandra* and *XMM-Newton* telescopes. Flux measurements agree to within  $3\sigma$  for 10 of the 12 spirals. For two red spirals, the flux differs by  $10.2\sigma$  and  $5.7\sigma$ .